

OPEN ACCESS

EDITED BY Yongzheng Chen,

Zunyi Medical University, China

REVIEWED BY

Ramesh Maruthi Chingle, National Institutes of Health (NIH), United States Xuefeng Li,

Southwest Minzu University, China

*CORRESPONDENCE

Peter Bai,

□ baip@med.unideb.hu

 Éva Bokor.

Bokor,
 Bokor.eva@science.unideb.hu

[†]These authors have contributed equally to this work and share first authorship

RECEIVED 29 April 2025 ACCEPTED 09 June 2025 PUBLISHED 01 September 2025

CITATION

Zaki AI, Sipos A, Kacsir I, Kovács NI, Kerekes É, Szoták E, Freytag C, Demény M, Révész I, Buglyó P, Bényei A, Janka EA, Kardos G, Somsák L, Bai P and Bokor É (2025) Platinumgroup metal half-sandwich complexes of 1-(α-D-glucopyranosyl)-4-hetaryl-1,2,3-triazoles: synthesis, solution equilibrium studies, and investigation of their anticancer and antimicrobial activities. *Front. Chem.* 13:1619991. doi: 10.3389/fchem.2025.1619991

COPYRIGHT

© 2025 Zaki, Sipos, Kacsir, Kovács, Kerekes, Szoták, Freytag, Demény, Révész, Buglyó, Bényei, Janka, Kardos, Somsák, Bai and Bokor. This is an open-access article distributed under the terms of the Creative Commons Attribution License (CC BY). The use, distribution or reproduction in other forums is permitted, provided the original author(s) and the copyright owner(s) are credited and that the original publication in this journal is cited, in accordance with accepted academic practice. No use, distribution or reproduction is permitted which does not comply with these terms.

Platinum-group metal half-sandwich complexes of $1-(\alpha-D-glucopyranosyl)-4-hetaryl-1,2,3-triazoles: synthesis, solution equilibrium studies, and investigation of their anticancer and antimicrobial activities$

Alshimaa I. Zaki^{1,2,3†}, Adrienn Sipos^{4†}, István Kacsir¹, Nóra Ildikó Kovács^{2,5}, Éva Kerekes⁴, Evelin Szoták⁶, Csongor Freytag⁶, Máté Demény⁴, István Révész⁴, Péter Buglyó⁵, Attila Bényei⁷, Eszter Anna Janka⁸, Gábor Kardos^{6,9,10}, László Somsák¹, Peter Bai^{4,11,12}* and Éva Bokor¹*

¹Department of Organic Chemistry, University of Debrecen, Debrecen, Hungary, ²Doctoral School of Chemistry, University of Debrecen, Debrecen, Hungary, ³Department of Chemistry, Faculty of Science, Mansoura University, Mansoura, Egypt, ⁴Department of Medical Chemistry, Faculty of Medicine, University of Debrecen, Debrecen, Hungary, ⁵Department of Inorganic and Analytical Chemistry, Faculty of Sciences and Technology, University of Debrecen, Debrecen, Hungary, ⁶One Health Institute, Faculty of Health Sciences, University of Debrecen, Debrecen, Hungary, ⁷Department of Physical Chemistry, Faculty of Sciences and Technology, University of Debrecen, Debrecen, Hungary, ⁸Department of Dermatology, Faculty of Medicine, University of Debrecen, Debrecen, Hungary, ⁹Department of Metagenomics, University of Debrecen, Debrecen, Hungary, ¹⁰National Public Health Centre, Budapest, Hungary, ¹¹NKFIH-DE Lendület Laboratory of Cellular Metabolism, Debrecen, Hungary, ¹²Research Center for Molecular Medicine, Faculty of Medicine, University of Debrecen, Debrecen, Hungary

Although platinum-based complexes are pivotal in chemotherapy, their clinical use is limited by toxicity and resistance. Previously, we identified a set of osmium, ruthenium, and iridium half-sandwich complexes of $1-N-(\beta-D-glucopyranosyl)-4$ -hetaryl-1,2,3-triazole-type N,N-chelators with potent and selective activity against a large set of diverse neoplasia cell models and multiresistant Grampositive bacteria (methicillin-resistant *Staphylococcus aureus* (MRSA) and vancomycin-resistant *Enterococcus* (VRE)). Our aim in this study was to assess how the configuration of the C1 carbon in the glucose moiety affects the biological activity of the complexes. Thus, $1-N-(\alpha-D-glucopyranosyl)-4$ -hetaryl-1,2,3-triazoles were synthesized and used as N,N-bidentate ligands to result in half-sandwich type complexes analogous to the earlier reported ones. Overall, the newly prepared complexes with the α -anomeric carbohydrate moiety had similar biological properties to the complexes with the β -anomeric carbohydrate unit in terms of their biological activity on cancer cells

or primary human cells. Importantly, the bacteriostatic property of the complexes with an α -anomeric sugar moiety was inferior to that of the complexes containing the β -anomer.

KEYWORDS

N-glycopyranosyl derivative, α -anomer, 1,2,3-triazole, half-sandwich complex, complex stability, cytostasis, bacteriostasis

1 Introduction

Platinum-based agents, as cisplatin, oxaliplatin, and carboplatin, represent pillars of chemotherapy regimens against numerous solid tumors and hematological malignancies (Kenny and Marmion, 2019; Yu et al., 2020; Zhang et al., 2022). Despite the versatility of the platins, their applicability is limited by platinum resistance and toxicity (Hartmann and Lipp, 2003; Mukherjea et al., 2020; McMullen et al., 2021; Sipos et al., 2021). This gap in the suitability of platins calls for the development of new organometallics (Boros et al., 2020; Bortolamiol et al., 2023; Singh et al., 2023; Omer et al., 2024) for which, among others, the complexes of other platinum-group metals (ruthenium (Melchart and Sadler, 2006; Hartinger et al., 2011; Zeng et al., 2017; Gichumbi and Friedrich, 2018; Meier-Menches et al., 2018; Coverdale et al., 2019; Kenny and Marmion, 2019; Štarha and Trávníček, 2019; Bashir et al., 2023; Prathima et al., 2023; Herić et al., 2024; Koziel et al., 2025), osmium (Hartinger et al., 2011; Hanif et al., 2014; Gichumbi and Friedrich, 2018; Konkankit et al., 2018; Meier-Menches et al., 2018; Štarha and Trávníček, 2019; Nabiyeva et al., 2020; Li et al., 2021; Prathima et al., 2023), iridium (Leung et al., 2013; Liu and Sadler, 2014; Gichumbi and Friedrich, 2018; Konkankit et al., 2018; Štarha and Trávníček, 2019; Prathima et al., 2023; Koziel et al., 2025; Mansour et al., 2025; Štarha, 2025), or rhodium (Leung et al., 2013; Gichumbi and Friedrich, 2018; Štarha and Trávníček, 2019; Máliková et al., 2021; Prathima et al., 2023; Saha et al., 2025)) appear to be potential candidates due to better toxicity profiles compared to platinum-based drugs (Mello-Andrade et al., 2018; Gano et al., 2019; Liu et al., 2019; Mihajlovic et al., 2020). In line with that, three ruthenium derivatives, NAMI-A (Leijen et al., 2015), KP1019/1339 (IT-139, BOLD100) (Burris et al., 2016), and TLD-1433 (Kulkarni et al., 2022) are already in various phases of clinical trials against neoplastic diseases such as bladder or lung cancer.

A subgroup of bioactive platinum-group metal complexes is the half-sandwich complexes with anticancer (Melchart and Sadler, 2006; Liu and Sadler, 2014; Gichumbi and Friedrich, 2018; Nabiyeva et al., 2020; Máliková et al., 2021; Bashir et al., 2023; Koziel et al., 2025; Mansour et al., 2025; Štarha, 2025) or even with antibacterial (Karpin et al., 2013; DuChane et al., 2018; Kljun et al., 2018; Lapasam et al., 2020a; Lapasam et al., 2020b; Lapasam et al., 2020c; Yufanyi et al., 2020; Bernier et al., 2021; Coverdale et al., 2021; Klaimanee et al., 2021; Balázs et al., 2022; Dimitrijevic et al., 2023; Kacsir et al., 2023a; Kacsir et al., 2023b), antiparasitic (Martínez et al., 2012; Desiatkina et al., 2020; Mbaba et al., 2020; Milheiro et al., 2020; Fandzloch et al., 2021; Holzer et al., 2022; Gambino, 2024), antiviral (Yufanyi et al., 2020; Chuong et al., 2021; Jankovic et al., 2022), and antifungal (Kljun et al., 2014; Klaimanee et al., 2021; Dimitrijevic et al., 2023) properties. We have recently synthesized a series of half-sandwich complexes with β-Dglycopyranosyl azole-type N,N-bidentate ligands and revealed their anticancer and antibacterial potentials (Kacsir et al., 2021; Balázs et al., 2022; Kacsir et al., 2023a).

Among them, the complexes of 1-N-(β -D-glucopyranosyl)-4hetaryl-1,2,3-triazoles (Figure 1A, I) proved to be the most promising subset with members (e.g., II in Figure 1A') displaying cytostatic properties with submicromolar IC50 values against a plethora of cellular models of various neoplasia (carcinomas, sarcomas and hematological malignancies), and also showing bacteriostatic activity with low micromolar MIC values on multiresistant Gram-positive bacteria (vancomycin-resistant Enterococcus (VRE) and methicillinresistant Staphylococcus aureus (MRSA)). In addition, these complexes, by exerting at least one order of magnitude lower IC₅₀ on cancer or bacterial cells than those values on human primary dermal fibroblasts, had definite selectivity (Kacsir et al., 2021; Balázs et al., 2022; Kacsir et al., 2022; Kacsir et al., 2023a). The complexes elicited oxidative stress in mammalian cells (Kacsir et al., 2021; Kacsir et al., 2022; Kacsir et al., 2023a) and in bacteria (Kacsir et al., 2023a), which could be a key process underlying their biological activity.

The main findings regarding the structure–activity relationships (SAR) of compounds I are outlined in Figure 1A (for details, the reader is kindly asked to survey our previous publications (Kacsir et al., 2021; Balázs et al., 2022; Kacsir et al., 2022; Kacsir et al., 2023a)). The most important feature regarding biological activity is the presence of *O*-protected (preferably *O*-perbenzoylated) carbohydrate moieties, which confer lipophilicity and likely facilitate cooperative target binding, while the removal of the protecting groups abolishes the biological activity of the complexes (Kacsir et al., 2021; Balázs et al., 2022; Kacsir et al., 2023a).

In this work, we will extend the SAR of **I** by an additional modification in the sugar part of the N,N-bidentate ligands (Figure 1B), namely, the application of 1-N-(α -D-glucopyranosyl)-4-hetaryl-1,2,3-triazoles (III) as ligands. The change of the anomeric configuration from β to α alters the orientation of the heterocyclic aglycon part of the glucose-derived N,N-chelators and that of the coordination sphere of the complexes. Thus, the main goal of this study is to assess how this modification in the molecular shape/geometry affects the biological effectiveness of this type of half-sandwich complex.

2 Results

2.1 Syntheses

The synthetic work was started with the preparation of the glucosederived N,N-bidentate ligands (Table 1). First, Cu(I)-catalyzed cycloaddition of *O*-peracetylated α-D-glucopyranosyl azide (Zhang et al., 1999) 1 with 2-ethynylpyridine and -quinoline was carried out

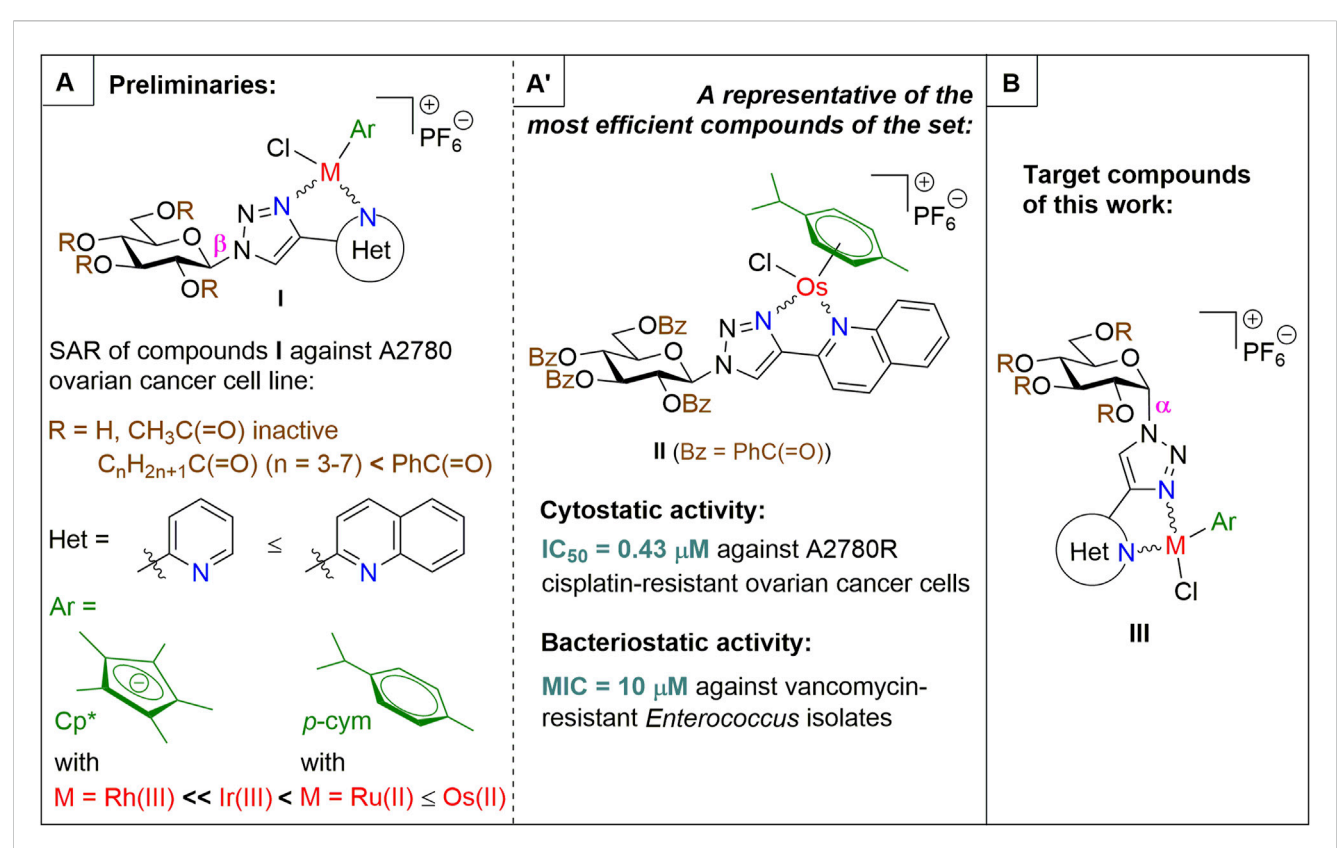


FIGURE 1

Outline of the SAR study for our previously published glucose-derived half-sandwich type complexes (A), a biologically active representative of the set (A'), and target compounds of the present work (B).

TABLE 1 Synthesis of 1-(α-D-glucopyranosyl)-4-hetaryl-1,2,3-triazoles.

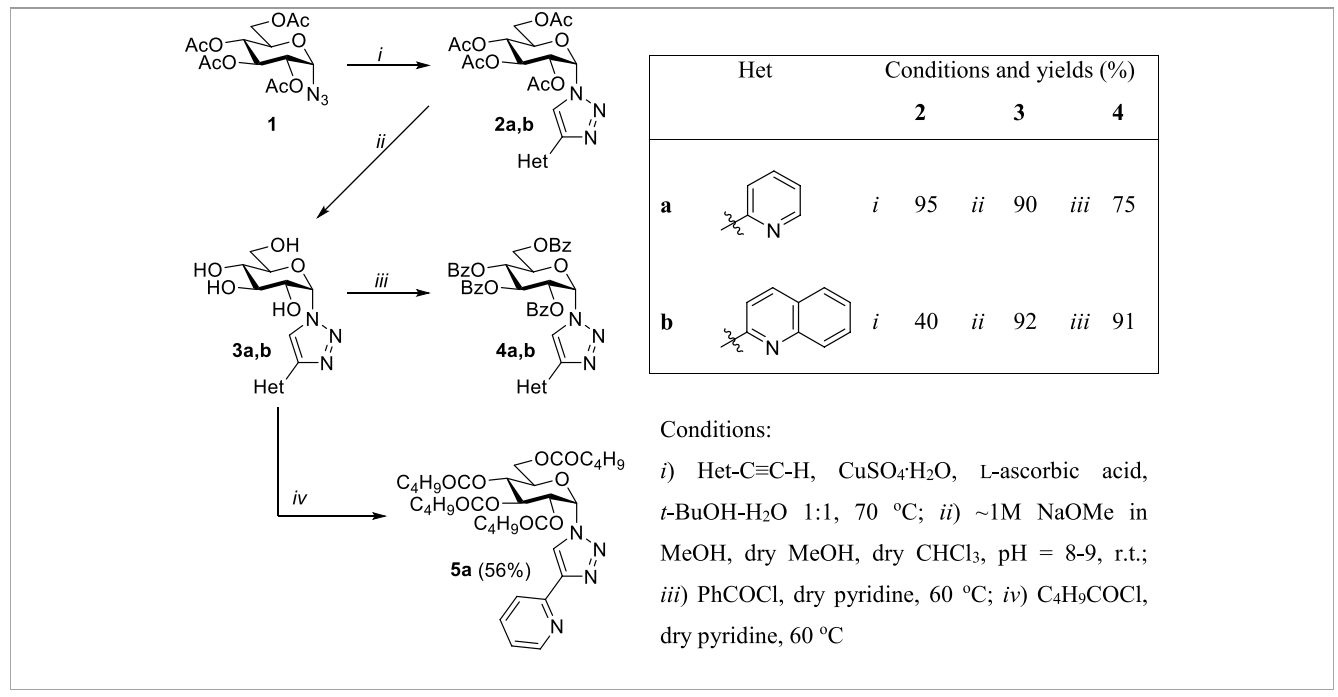
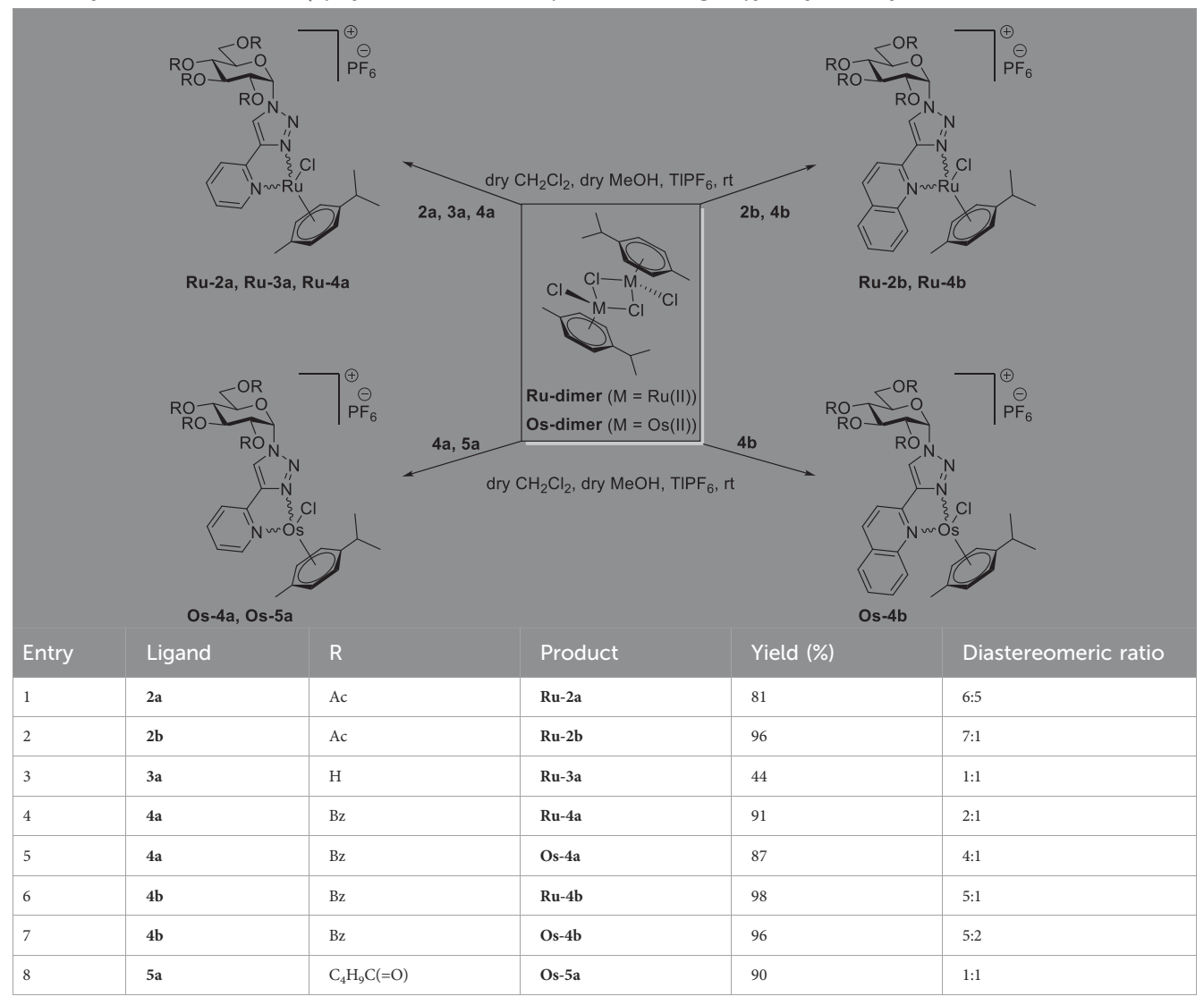


TABLE 2 Synthesis of half-sandwich $(\eta^6-p-\text{cym})\text{Ru}(II)$ and -Os(II) complexes with 1- $(\alpha-p-\text{glucopyranosyl})$ -4-hetaryl-1,2,3-triazoles.



under standard CuAAC conditions (Wilkinson et al., 2006; Kraft et al., 2015), using a CuSO_4/L -ascorbic acid catalyst system in aqueous tert-butyl alcohol to get O-peracetylated 1-(α -D-glucopyranosyl)-4-hetaryl-1,2,3-triazoles ($2\mathbf{a}$, \mathbf{b}) in moderate to high yields. Compounds $2\mathbf{a}$, \mathbf{b} were subsequently subjected to Zemplén deacetylation to afford the unprotected derivatives $3\mathbf{a}$, \mathbf{b} in excellent yields. Treatment of $3\mathbf{a}$, \mathbf{b} with benzoyl chloride in pyridine resulted in the corresponding O-perbenzoylated analogs $4\mathbf{a}$, \mathbf{b} in high yields. Additionally, the hydroxyl groups of compound $3\mathbf{a}$ were esterified by pentanoyl chloride to obtain ligand $5\mathbf{a}$ in acceptable yield.

With the new glucose-based heterocyclic ligands in our hands, the synthesis of the target complexes, by the adaptation of our earlier published method (Kacsir et al., 2021; Kacsir et al., 2022; Kacsir et al., 2023a), was the next step (Table 2 and Table 3).

Accordingly, the 2-pyridyl substituted 1,2,3-triazoles 2a-5a were reacted with dichloro (η^6 -p-cymene)Ru(II) and -Os(II) dimers (**Ru-dimer** and **Os-dimer**) in the presence of TlPF₆ in a mixture of CH₂Cl₂ and MeOH (Table 2) to give the desired cationic half-sandwich type Ru(II) and Os(II) complexes **Ru-2a-Ru-4a** (entries 1,3,4), **Os-4a** (entry 5), and **Os-5a** (entry 8) with a PF₆⁻

counterion. Treatment of the 2-quinolyl derivatives **2b** and **4b** with the same chloro-bridged dimers was also performed (Table 2), resulting in further *p*-cymene-containing complexes **Ru-2b** (entry 2), **Ru-4b** (entry 6), and **Os-4b** (entry 7).

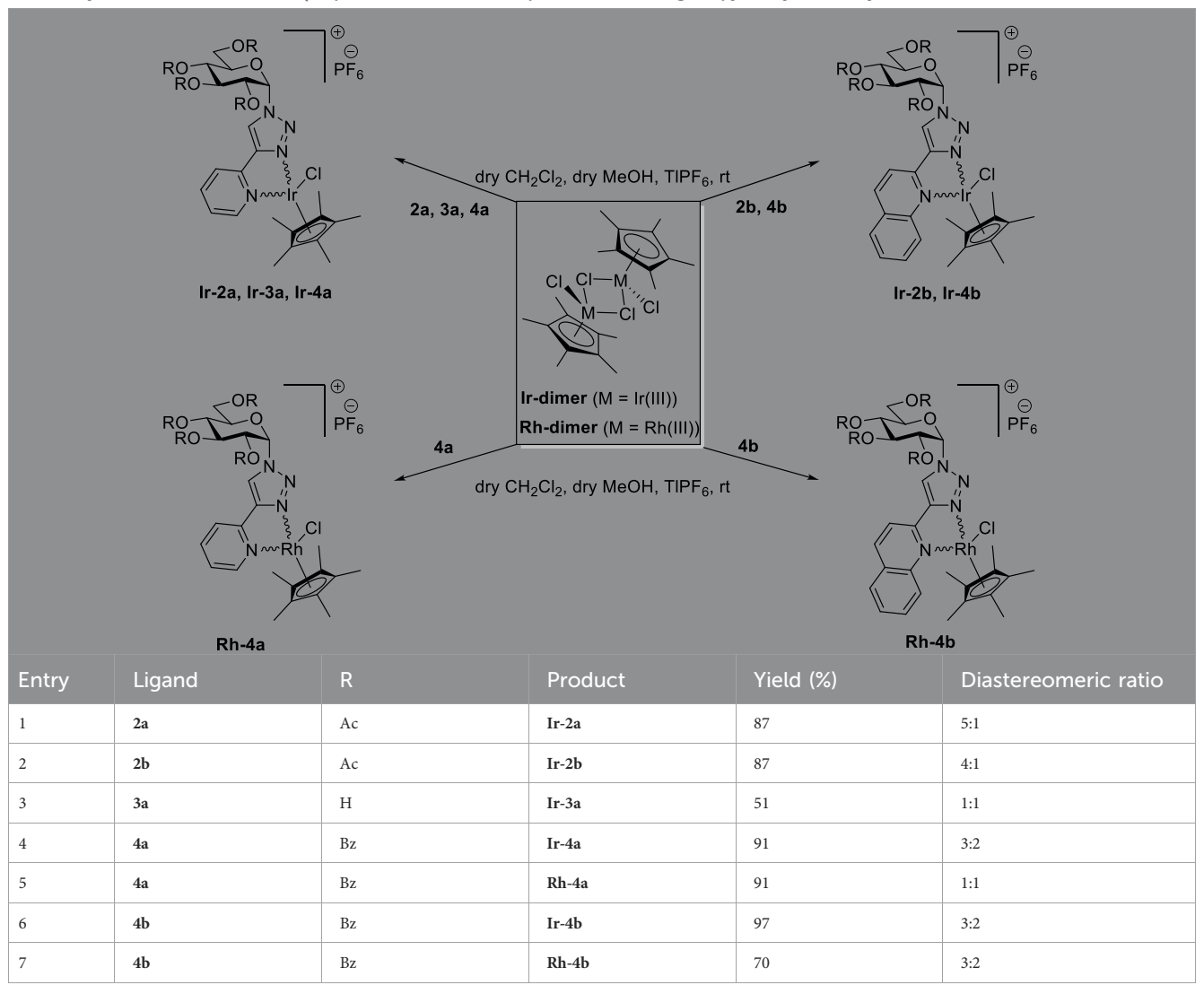
The complexation of the above ligands was also accomplished with dichloro (η^5 -pentamethylcyclopentadienyl)Ir(III) and Rh(III) dimers (**Ir-dimer** and **Rh-dimer**, **Table 3**) furnishing half-sandwich- type (η^5 -Cp*)Ir(III) complexes **Ir-2a,b** (entries 1 and 2), **Ir-3a** (entry 3), **Ir-4a,b** (entries 4 and 6), and Rh(III)-based analogs **Rh-4a,b** (entries 5 and 7).

Similar to previously reported complexes with 1-(β -D-glucopyranosyl)-4-hetaryl-1,2,3-triazoles (Kacsir et al., 2021; Kacsir et al., 2022; Kacsir et al., 2023a), all of the newly prepared complexes presented in Tables 2 and 3 were obtained as mixtures of two diastereoisomers.

2.2 X-ray structure of complex Ir-3a

A single crystal of one of the isomers of **Ir-3a** could be obtained by slow evaporation of the solution of the corresponding complex in

TABLE 3 Synthesis of half-sandwich $(\eta^5-Cp^*)Ir(III)$ and -Rh(III) complexes with $1-(\alpha-p-glucopyranosyl)-4-hetaryl-1,2,3-triazoles.$

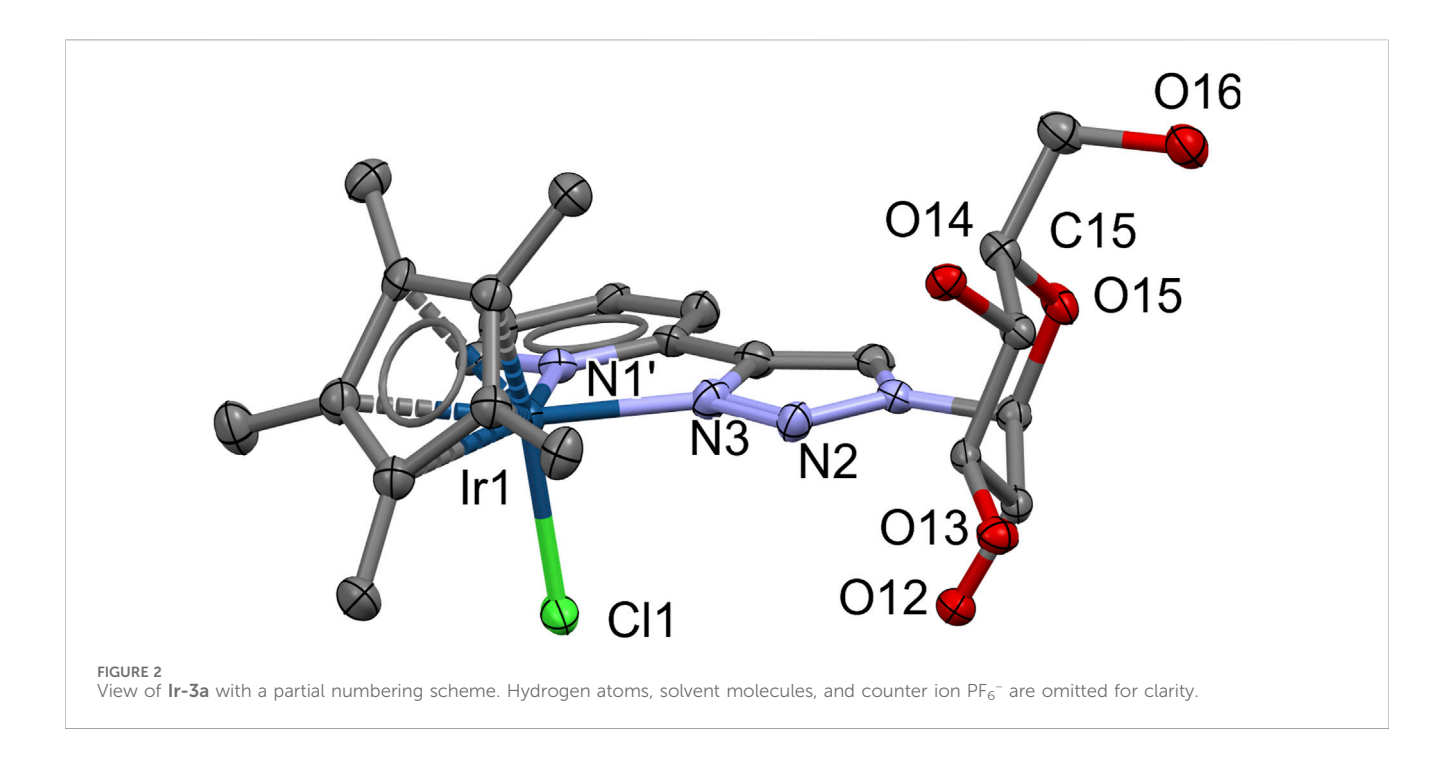


i-propyl alcohol at room temperature. The X-ray crystallography analysis of this sample confirmed the presumed coordination mode with the 5-membered chelate ring formed by the assistance of the glucose-based heterocyclic N,N-bidentate ligand **3a** (Figure 2). The asymmetric unit, apart from the PF₆⁻ counterion, contains *i*-propyl alcohol and two water molecules. The coordination of the complex is the expected one. For example, the angle between the plane of the Cp* ring and the (Ir,N,N) plane is 57 degrees, which is in good agreement with other similar structures found in the Cambridge Structural Database. Moreover, the sugar moiety and the pyridinyl-triazole ring system make an L-shape, as can be seen in Figure 2. CCDC deposition number: 2440135 for **Ir-3a** contains the supplementary crystallographic data for this article.¹

2.3 Interaction of ligands 3a and 3b with $[(\eta^6-p\text{-cym})Ru]^{2+}$ and $[(\eta^5\text{-Cp*})Rh]^{2+}$ cations in solution

In order to obtain information on the acidbase character of the ligands and on the stoichiometry and stability of the complexes present in aqueous medium, potentiometric titrations were carried out in selected systems. Based on the results, both 3a and 3b, having good enough solubility in water, are capable of releasing one hydrogen ion from the fully protonated forms in the measurable pH range (see Figure 3, "pK"). The calculated pK_a values appear in Table 4; these values belong to the N-heterocyclic ring of the ligands. The slightly lower values compared to those of the parent N-donors (pyridine: 5.25 (Chmurzyński, 2000), quinoline: 4.93 (Wu et al., 1995)) can be interpreted by the close vicinity of the triazole rings making the pyridine or quinoline N-s less basic in these novel ligands, even though an internal hydrogen bond formation is possible. For comparison, the previously prepared β-anomeric pair of 3a, compound 3a-β (Kacsir et al., 2021) in Table 4, was also studied. Notably, there is no significant difference in the acidbase character of the two anomers (Table 4).

¹ These data can be obtained free from www.ccdc.cam.ac.uk/data_request/cif, or by emailing data_request@ccdc.cam.ac.uk, or by contacting The Cambridge Crystallographic Data Centre, 12 Union Road, Cambridge CB2 1EZ, UK; fax: +44 1223 336033.



Because the studied organoosmium and -iridium cations are known to form complexes in slow processes, they were not suitable for direct pH-potentiometric titrations. Complexes containing the $[(\eta^6-p\text{-cym})Ru]^{2+}$ entity were found to be active in previous biological studies (Kacsir et al., 2021; Kacsir et al., 2022; Kacsir et al., 2023a; Kacsir et al., 2023b). Therefore, solution equilibrium studies were first performed in the presence of this metal ion. Representative titration curves are shown in Figure 3A. With this metal ion, reaching pH equilibrium was also found to be a very slow process; under the measuring conditions, no steady data points could be obtained. At the same time, the tentative curves indicate a moderate pH effect of the metal ion that can be seen in the acidic pH range due to the low basicity of the ligands. Above pH ~ 7.0, however, extra base consumption processes occur, presumably due to partial hydrolysis of the metal ion. Due to uncertain data points, the titration curves registered in the organoruthenium samples could not be evaluated.

Although its complexes did not exhibit considerable activity either, to model the solution equilibrium processes, the organorhodium ion was also involved in these studies. In this case, a smaller pH effect was observed in the acidic pH range (Figure 3B); however, unlike the organoruthenium system, no hydrolysis of the metal ion is noticeable in the range 5.5 < pH < 9.0, revealing the presence of complexed species only. Evaluation of the titration curves in the range 2.0 < pH < 7.0 resulted in very simple models with a single complex, [ML]²⁺, in which the (N,N) coordination of the ligands is assumed. Comparing the two metal ion containing systems, the complexation with $[(\eta^6-p-\text{cym})\text{Ru}]^{2+}$, starts at a more acidic pH, but hydrolytic processes occur already in the physiological pH range due to the higher affinity of the metal ion to hydrolysis. For the $[(\eta^5-Cp^*)Rh]^{2+}$, these processes are shifted towards higher pH; therefore, the [RhL]2+ species is still present at physiological pH. The rather similar values of the [RhL] complexes (Table 4) for the three ligands may indicate that the presence of the

second aromatic ring in 3b and the orientation of the triazole ring for pyridine-containing ligands (3a and 3a- β) have no significant effect on the stability of the chelate formed with the metal ion.

2.4 Biological characterization of the complexes

2.4.1 The complexes do not exert rapid toxicity but impair mitochondrial respiration

The first step in the biological characterization of the complexes was the screening for the capacity of the complexes to exert rapid toxicity, that is, cell death, using the MTT assay. None of the ligands (2a, 2b, 3a, 4a, 4b, 5a) induced toxicity in ovarian cancer cells (A2780 and ID8 cells) or human primary dermal fibroblasts (Figures 4, 5; Table 5). Complexes in which the hydroxyl groups of the carbohydrate moiety were unprotected or esterified by acetyl groups (Ru/Ir-2a,b, Ru/Ir-3a) did not induce cell death in A2780 cells in accordance with our previous observations (Kacsir et al., 2021; Kacsir et al., 2022; Kacsir et al., 2023a; Kacsir et al., 2023b) (Figure 4; Table 5). However, complexes of the O-perbenzoylated ligands 4a and 4b or the O-perpentanoylated ligand 5a, to our surprise, induced MTT reduction that is a sign of acute toxicity in ovarian cancer cells (A2780 and ID8 cells), as well as in the untransformed human primary dermal fibroblasts (Figure 5; Table 5). This finding contrasted with our previous observations as the complexes with the β-configured glucose moiety did not induce toxicity (Kacsir et al., 2021; Kacsir et al., 2022; Kacsir et al., 2023a). Namely, the ruthenium, osmium, and iridium complexes of ligands 4a, 4b, and 5a (Ru/Os/Ir-4a,b, Os-5a) induced acute toxicity, while the rhodium complexes of ligands 4a and 4b (Rh-4a, Rh-4b) did not have such property on either of the cell lines assessed (Figure 5; Table 5).

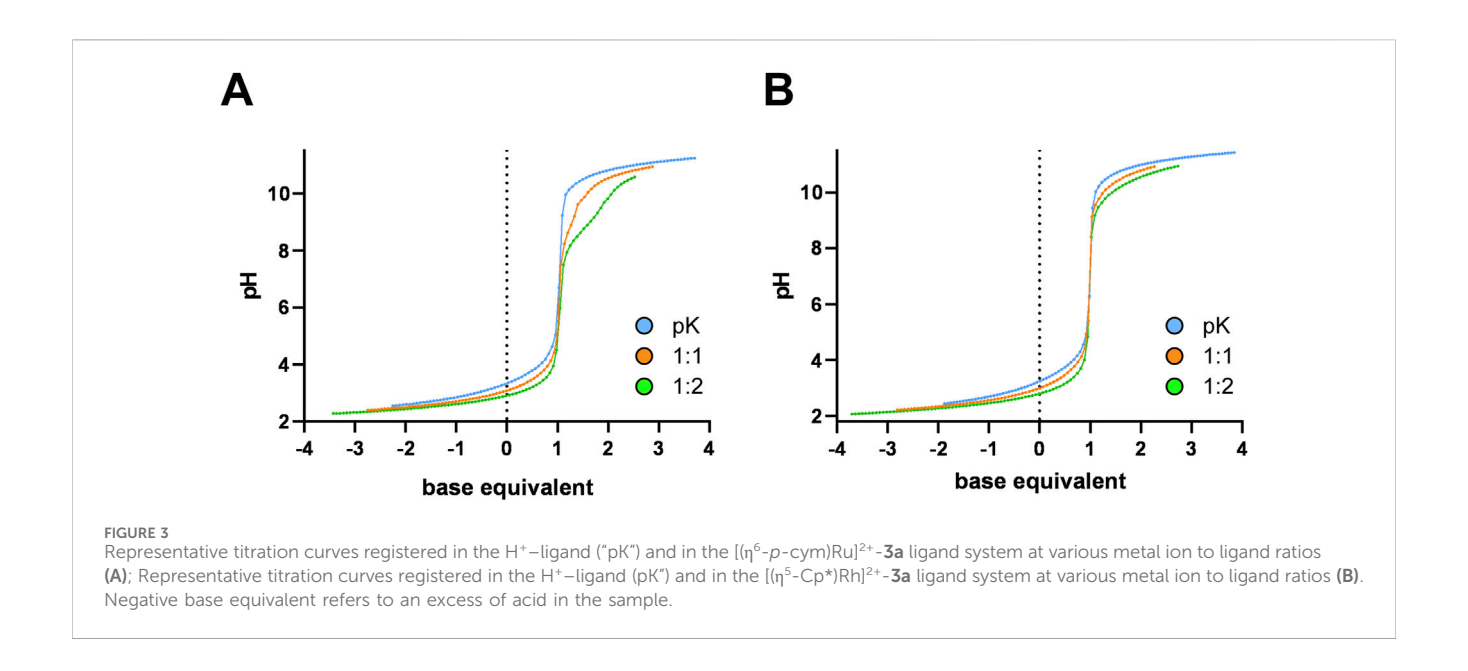


TABLE 4 Protonation constants (pK_a) of the ligands studied and stability constants $(\log \beta)$ of the ML complexes with the $[(\eta^5-\text{Cp*})\text{Rh}]^{2+}$ metal ion.

		,	
Ligand	HO HO N N	HO HO N N	HO OH N=N
	3a	3b	3a -β (Kacsir et al., 2021)
pK_a	3.59 (1)	3.56 (1)	3.44 (2)
		$[(\eta^5\text{-}Cp^\star)Rh]^{\scriptscriptstyle 2+}$	
${ m log}eta_{ m [ML]}$	5.50 (4)	5.55 (3)	5.12 (2)

To verify the toxicity-inducing behavior of the complexes with β (non-toxic) and α (slightly toxic) anomeric sugar moiety, we complemented the MTT assay with the propidium iodide-annexin V-FITC double staining in case of the complexes that efficiently reduced the MTT signal in A2780 or primary fibroblast cells (complexes of ligands 4a, 4b, and 5a). All compounds were applied in concentrations corresponding to the IC50 value obtained in MTT assays and in SRB assays (SRB assays are discussed later) on A2780 cells and primary human dermal fibroblasts. Assessing these concentrations ensured that we could detect acute toxicity in concentrations that induced long-term cytostasis. From our perspective, it was not important to distinguish between apoptosis and necrosis. We summed up propidium iodide, annexin V, and double-positive cells as dead cells and contrasted them with double-negative (living) cells. Importantly, the active complexes of 4a, 4b, and 5a induced only marginal cell death (Figure 6) that was comparable to

previous observations with the complexes of ligands incorporating a β -D-glucopyranosyl moiety (Kacsir et al., 2021; Kacsir et al., 2023a; Kacsir et al., 2023b).

2.4.2 Complexes with benzoyl- and pentanoylprotected glucose units have selective cytostatic properties

We assessed the cytostatic properties of the complexes using the sulforhodamine B (SRB) assay (Skehan et al., 1990). None of the free ligands (2a,b, 3a, 4a,b, 5a) proved to be cytostatic on any of the cell lines used in the study (Figures 4, 7; Table 5). Similar to the toxicity results, complexes in which the OH-groups of the glucose moiety were not protected (Ru/Ir-3a) or were *O*-peracetylated (Ru/Ir-2a,b) did not exert cytostasis (Figure 4; Table 5). In contrast to that, complexes containing *O*-perbenzoylated (Ru/Os/Ir-4a,b) or -pentanoylated (Os-5a) sugar units exerted cytostasis in all cell lines (Figure 7). Of the *p*-cym-Ru(II), *p*-cym-Os(II), and Cp*-

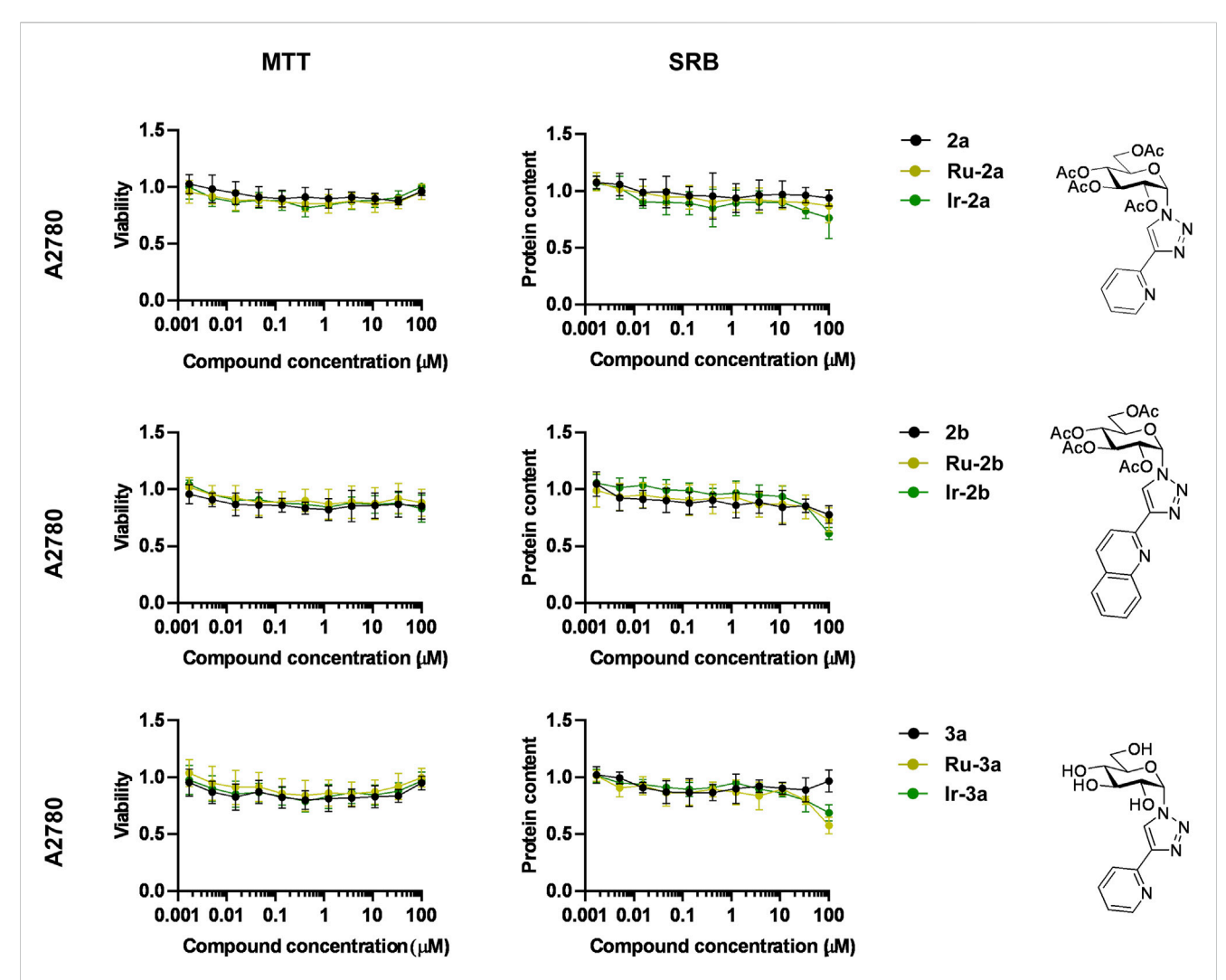
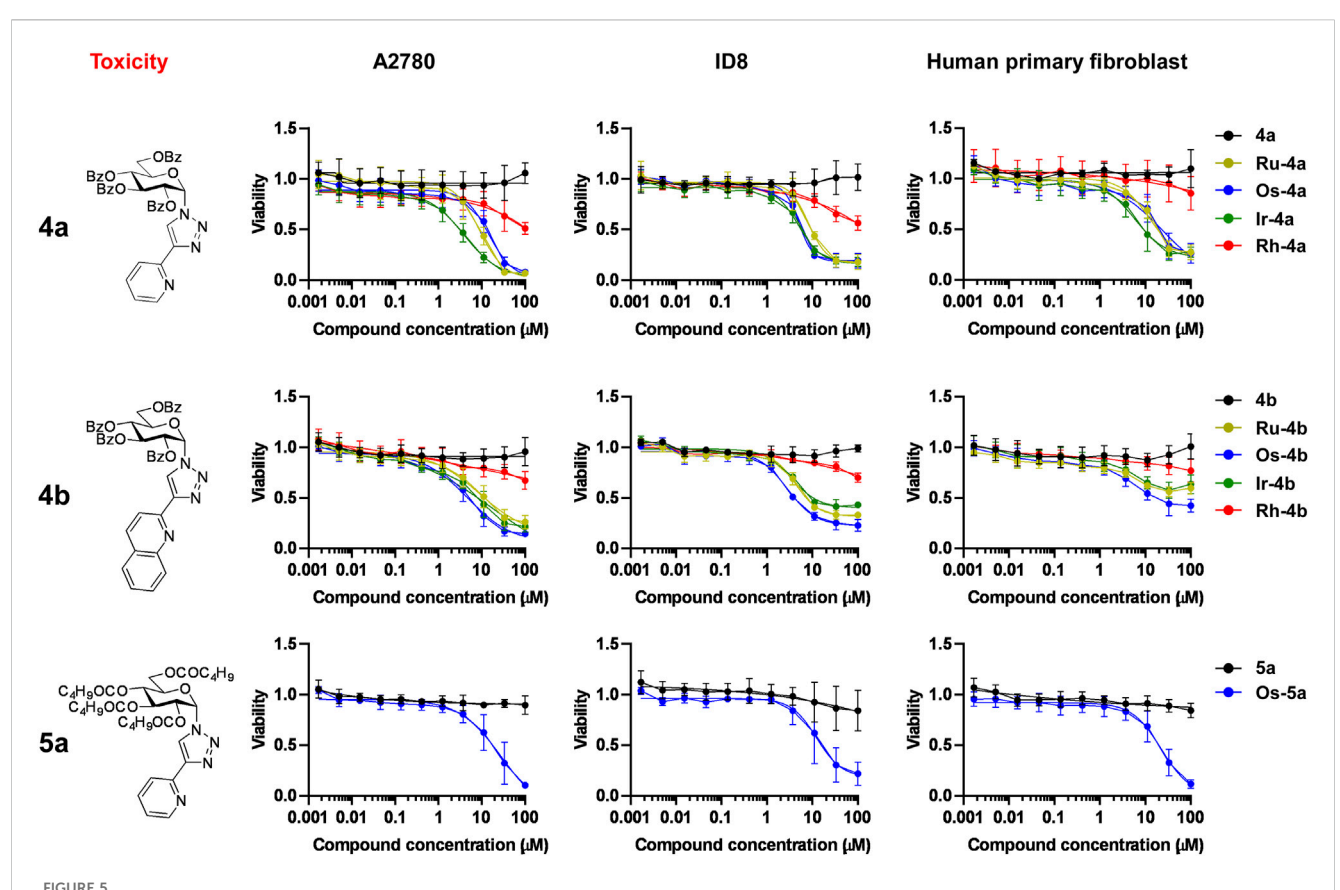


FIGURE 4
The ruthenium and iridium complexes of ligands 2a, 2b, and 3a do not influence cell viability and cell proliferation. For MTT assays, 4×10^3 A2780 cells were plated into 96-well plates, and for SRB assays, 1.5×10^3 A2780 cells were plated into 96-well plates. Cells were treated with the compounds in the concentrations indicated for either 4h for an MTT assay or for 48h for an SRB assay. Data are represented as average \pm SD, from four biological replicates, with the exception of the MTT dataset of 1r-2b and the SRB datasets of 2b, 1r-2b, and 1r-3a, which were derived from three biological replicates. Individual assays were performed in duplicate. Values were normalized for vehicle-treated cells, and the absorbance for vehicle-treated cells equals 1. Data are represented as fold change compared to vehicle-treated controls. Normality was assessed using the D'Agostino-Pearson test. Statistical significance was assessed using a two-way ANOVA test followed by Tukey's post hoc test. For better visibility, normality, transformations, statistical tests, and p values are presented in an MS Excel sheet at https://figshare.com/s/3a0aa60b66f3f746f41e. Nonlinear regression was performed on the datasets; $1C_{50}$ values are indicated in Table 5. Color code: black—free ligand 12a, khaki—ruthenium complex 11r-3a.

Ir(III) and Cp*-Rh(III) complexes of **4a** and **4b** (**Ru/Os/Ir/Rh-4a,b**), the latter ones (**Rh-4a,b**) were markedly less efficient or were ineffective compared to their counterparts **Ru/Os/Ir-4a,b** in all model systems (**Figure 7**). The IC₅₀ values of the *p*-cym-Ru(II), *p*-cym-Os(II), and Cp*-Ir(III) complexes of ligands **4a**, **4b**, and **5a** were in the low micromolar-to-submicromolar range in both A2780 and ID8 ovarian cancer cells (**Figure 7**; **Table 5**). The quinoline-containing complexes (complexes of **4b**) had better IC₅₀ values than their pyridine-containing pairs (complexes of **4a** and **5a**) (**Figure 7**; **Table 5**). Importantly, the IC₅₀ values of the same complexes on primary human dermal fibroblasts were one order of magnitude higher than their IC₅₀ values on A2780 and ID8 ovarian cancer cells (**Figure 7**; **Table 5**), suggesting a reasonable therapeutic index.

2.4.3 The bioactive complexes have cytostatic properties on a larger set of neoplasias, similar to their cytostatic properties on primary human fibroblasts

Next, we investigated whether the bioactive complexes would be active against a larger set of neoplasias. This set of cells was selected to include another carcinoma (Capan2, a pancreatic adenocarcinoma), a sarcoma (U2OS, an osteosarcoma), and a lymphoma (L428, a Hodgkin lymphoma) cell line. Similar to the results on ovarian cancer cell lines, the complexes previously identified to possess cytostatic activity (Ru/Os/Ir-4a,b, Os-5a) proved to be active on these models, too (Figure 8). Another important difference between the activity of the complexes on A2780 and ID8 cells versus on Capan-2 and U2OS cells was the



The ruthenium, osmium, and iridium complexes of ligands 4a, 4b, and 5a decrease MTT reduction. For MTT assays, 4×10^3 A2780 cells, 3×10^3 ID8 cells, or 6×10^3 human primary fibroblasts were plated into 96-well plates. Cells were treated with the compounds in the concentrations indicated for 4 h. Data are represented as average \pm SD, from four biological replicates on A2780, and from three biological replicates on ID8 and human primary fibroblasts. For the datasets of 5a and 6a-6a-6a on human primary fibroblasts, the data represent four biological replicates. Individual assays were performed in duplicate. Values were normalized for vehicle-treated cells, and the absorbance for vehicle-treated cells equals 1a. Normality was assessed using the D'Agostino-Pearson test. Statistical significance was assessed using a two-way ANOVA test followed by Tukey's post hoc test. For better visibility, normality, transformations, statistical tests, and p values are presented in an MS Excel sheet at https://figshare.com/s/3a0aa60b66f3f746f41e. Nonlinear regression was performed on the datasets; IC50 values are indicated in Table 5a. Color code: black—free ligand (5a, 5a), khaki—ruthenium complex (6a, 6a), green—iridium complex (6a, 6a), blue—osmium complex (6a, 6a), and red—rhodium complex (6a, 6a), blue—osmium complex (6a, 6a), and red—rhodium complex (6a, 6a).

narrowing of the therapeutic index (IC_{50} value on the cancer cell line vs IC_{50} value on primary human dermal fibroblasts), likely limiting the possible use of these complexes in diseases other than ovarian cancer.

2.4.4 The bioactive complexes have cytostatic properties on cisplatin-resistant A2780 cells

Cisplatin-resistance is a factor frequently limiting the complete delivery of platinum-based therapy (McMullen et al., 2021; Sipos et al., 2021); therefore, we assessed whether these complexes can induce cytostasis in cisplatin-resistant A2780 cells. The cisplatin-resistant cells were purchased from Sigma-Aldrich, and we characterized these cells in one of our previous studies (Kacsir et al., 2023a). The difference in the IC₅₀ values of the cisplatin-sensitive versus the cisplatin-resistant cells to cisplatin was 13.6-fold (1.21 μ M \rightarrow 16.47 μ M). Rhodium complexes were excluded from the investigation as their activity on A2780 cells was negligible (Figure 7; Table 5).

The ruthenium(II), osmium(II), and iridium(III) complexes of $\bf 4a$, $\bf 4b$, and $\bf 5a$ exerted cytostatic activity on the cisplatin-resistant A2780 cells with somewhat elevated IC₅₀ values that were similar to

the IC_{50} values of the cisplatin-sensitive A2780 cells (Figure 9; Table 5). With regards to the MTT assays, the ruthenium(II), osmium(II) and iridium(III) complexes of 4a, 4b, 5a did not affect MTT reduction (Figure 9; Table 5), in contrast to their effects on A2780 cells or human primary fibroblasts (Figure 7; Table 5).

2.4.5 Bioactive complexes exert cytostasis through inducing oxidative stress

Previous data evidenced that complexes with a similar structure induce oxidative stress in mammalian cells and in bacteria (Xu et al., 2018; Fernandes, 2019; Bakewell et al., 2020; Mihajlovic et al., 2020; Kacsir et al., 2021; Kacsir et al., 2022; Kacsir et al., 2023a; Kacsir et al., 2023b), suggesting that the α-anomer complexes discussed in the current manuscript may also act through eliciting oxidative stress. To study that, we applied vitamin E to scavenge reactive oxygen species (ROS). Vitamin E treatment led to a rightward shift in the sigmoid inhibitory curve of the complexes Ru/Os/Ir-4a,b, Os-5a (Figure 10), among which only Ru-4a, Os-4b showed a trend but lacked statistical significance. These observations suggest that ROS scavenging by vitamin E protects against the cytostatic property of

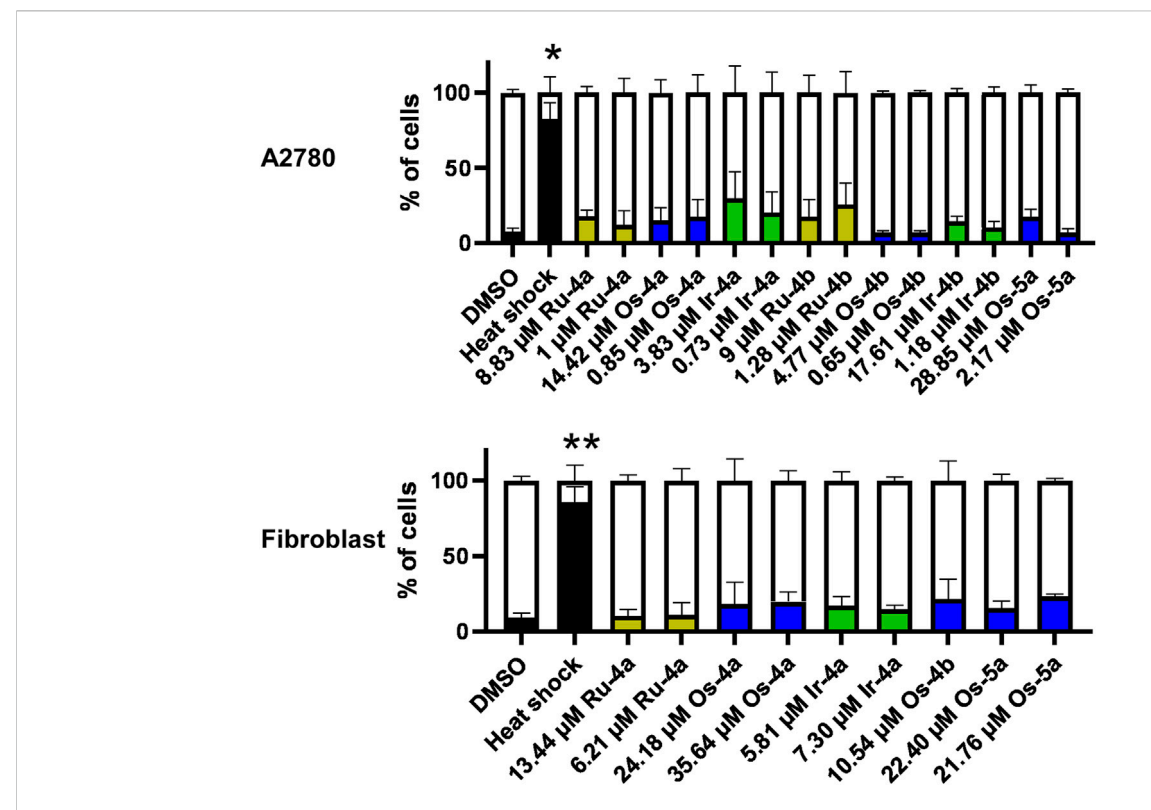


FIGURE 6
The ruthenium, osmium, and iridium complexes of ligands 4a, 4b, and 5a do not induce cell death. For the assay, 2×10^6 A2780 cells or 8×10^5 fibroblasts were plated into 12-well plates and were treated with the indicated complexes at the indicated concentrations for 4 h. Cells undergoing heat shock were used as the positive control. Cells were then stained with annexin V and propidium iodide (PI) and subjected to flow cytometry as described in *Materials and Methods*. The percentage of cells in the double negative quadrant (in the white part of the bar) and the sum of the remaining three quadrants (i.e., dead cells; filled part of the bar) are depicted. Data are represented as average \pm SD, from three biological replicates. Statistical analysis was performed on the proportion of dead cells in each sample set, comparing treatments to the vehicle (DMSO) control. Normality was assessed using the Shapiro-Wilk's test, and the Kruskal-Wallis test was applied, followed by Dunn's post hoc test. * and ** symbolize statistically significant differences between the indicated cohort and the DMSO-treated cells at p < 0.05 or 0.01, respectively. Color code: black—DMSO-treated or heat-shocked cells, khaki—ruthenium complex (**Ru-4a,b**), green—iridium complex (**Ir-4a,b**), and blue—osmium complex (**Os-4a,b** or **Os-5a**).

the complexes. Vitamin E has an apolar phytyl chain, rendering the whole molecule apolar and prone to protect biomembranes from oxidation (Hon-Wing et al., 1981). Trolox, a version of vitamin E without the apolar phytyl chain, does not have a protective effect on cells treated with the complexes of the same structure but with a β -anomeric glucose moiety (Kacsir et al., 2021). These suggest that the complexes likely induce the oxidation of biomembranes and/or elicit pathways that stem from oxidized biomembranes (e.g., chaperone-induction (Horváth et al., 1998; Gombos et al., 2011).

2.4.6 Bioactive ruthenium(II), osmium(II), and iridium(III) complexes have limited bacteriostatic activity

Previously, we showed that other half-sandwich complexes with a similar structure have bacteriostatic properties on sensitive and multiresistant isolates of Gram-positive species such as *Staphylococcus aureus* and *Enterococcus faecalis* or *E. faecium* (Balázs et al., 2022; Kacsir et al., 2023a; Kacsir et al., 2023b). Along the same lines, we tested the bioactive members of the newly prepared complexes on a reference strain and clinical isolates of *Staphylococcus aureus* and *Enterococcus faecium*. Our earlier observation for analogous complexes was that only those complexes that possessed antibacterial features

which had cytostatic properties on mammalian cancer cells. For that reason, we applied only those complexes of the new set that were cytostatic on A2780 cells, namely, Ru/Os/Ir-4a,b and Os-5a.

The MIC values determined for the reference strain of *S. aureus* were in the range of 5–40 μ M, whereas those for *E. faecalis* were in the range of 5–20 μ M, and both reference strains were sensitive to all of the studied complexes (Figure 11; Table 6). In contrast, not all clinical isolates were sensitive to all complexes. In case of the MRSA and VRE clinical isolates, complexes with *O*-perbenzoylated sugar moiety (Ru/ Os/Ir-4a,b) were not bacteriostatic on all isolates in contrast to Os-5a, which has a pentanoylated sugar unit (Figure 11; Table 6). The MIC values of the effective complexes were similar to or better than the MIC values on the reference strains (Figure 11; Table 6).

3 Discussion

In this study, we assessed the antineoplastic and antimicrobial potential of platinum-group metal half-sandwich complexes of α -D-glucopyranosyl 1,2,3-triazole-type ligands. The most important observations demonstrated that 1) the lipophilic character of the complexes, triggered by suitable $\it O$ -protection of

TABLE 5 The distribution coefficients (logD), the maximal inhibitory, IC_{50} , and Hill coefficient values of the complexes. n.c. – cannot be calculated.

		A2780						ID8					Fibroblast						
			МТТ		SRB		МТТ		SRB		MTT			SRB					
	logD	max %	IC50 (µM)	Ħ	max %	IC50 (μΜ)	\ \ \ \ \ \ \ \ \ \ \ \ \ \ \ \ \ \ \	max %	ICso (µM)	Ī	max %	IC50 (µM)	Ħ.	max %	ICso (µM)	Ħ	max %	IC50 (µM)	Ħ
2a		0			0														
Ru-2a	-2.13	0			0														
Ir-2a	-1.77	0			0														
2b		0			22.33														
Ru-2b	-1.15	0			26.98														
Ir-2b	-0.91	0			38.84														
3a		0			0														
Ru-3a	-1.96	0			42.35														
Ir-3a	-2.53	0			31.25														
4a		0			29.51			0			0			0			11.89		
Ru-4a	+1.88	>90	8.83	1.51	>90	1	1.98	82.06	8.12	2.12	>90	3.73	2.17	71.00	12.67	1.36	89.13	6.36	2.07
Os-4a	+1.67	>90	14.42	1.57	>90	0.85	1.91	80.66	5.01	2.77	>90	3.11	n.c.	73.90	24.18	0.79	87.90	35.64	0.91
Ir-4a	+1.87	>90	3.83	1.06	>90	0.73	1.73	82.08	4.99	1.71	>90	2.13	2.73	72.70	5.81	1.23	82.44	7.30	1.71
Rh-4a	+1.79	48.92			>90	n.c	n.c.	43.68			0			14.61			0		
4b		0			0			0			0			0			10.76		
Ru-4b	+1.61	73.80	9.00	0.78	>90	1.28	1.84	66.85	4.31	1.73	>90	1.38	2.30	43.85			64.73	12.40	2.61
Os-4b	+1.39	85.32	4.77	0.85	>90	0.65	1.94	77.24	2.80	1.37	>90	0.93	3.51	57.66			84.53	10.54	2.71
Ir-4b	+1.89	78.26	17.61	0.43	>90	1.18	1.71	58.48	3.50	1.46	>90	n.c.	n.c.	42.41			47.88		
Rh-4b	+1.64	32.64			75.23			30.06			0			23.08			0		
5a		0			33.92			15.89			0			15.72			27.97		
Os-5a	+1.97	>90	28.85	0.88	>90	2.17	1.86	78.16	12.39	1.55	>90	4.92	3.44	88.29	22.4	1.35	>90	21.76	2.47

TABLE 5 (Continued) The distribution coefficients (logD), the maximal inhibitory, IC₅₀, and Hill coefficient values of the complexes. n.c. – cannot be calculated.

	Capan2 SRB			U2OS SRB			L428 SRB			Cisplatin-resistant A2780					
										MTT			SRB		
	max %	ICso (µM)	H H	max %	ICso (µM)	Ħ	max %	ICso (µM)	Ħ	max %	ICso (µM)	Ħ	max %	IC50 (µM)	Ħ
2a															
Ru-2a															
Ir-2a															
2b															
Ru-2b															
Ir-2b															
3a															
Ru-3a															
Ir-3a															
4a															
Ru-4a	>90	2.60	3.30	>90	9.07	2.95	88.72	17.16	2.50	74.47	11.43	1.46	>90	2.70	2.66
Os-4a	>90	2.09	1.64	>90	10.8	3.08	>90	19.76	3.56	48.49	n.c.	n.c.	>90	1.99	2.40
Ir-4a	>90	1.99	2.35	>90	6.58	2.99	87.35	n.c.	n.c.	75.69	8.08	1.97	>90	2.43	3.43
Rh-4a	47.71			0			52.46			31.38			74.37	n.c.	n.c.
4b															
Ru-4b	>90	2.20	2.91	88.19	4.26	3.07	>90	2.64	2.42	19.79			>90	3.57	2.63
Os-4b	>90	0.96	2.24	>90	3.65	2.66	>90	n.c.	n.c.	40.32			>90	2.56	2.43
Ir-4b	>90	1.45	2.15	>90	4.98	1.98	>90	n.c.	n.c.	25.35			>90	2.88	2.13
Rh-4b	61.73			0			>90	6.36	0.92	0			30.30		
5a															
Os-5a	>90	5.25	2.85	>90	20.40	2.05	>90	5.10	3.40	68.17			86.36	3.63	3.30

the sugar moiety, is a prerequisite for their biological activity: complexes of the unprotected and O-peracetylated glucosederived ligands 2a,b and 3a with negative logD values were ineffective, while the use of larger, aromatic (benzoyl) or openchain (pentanoyl) acyl protection in the sugar part (4a,b, 5a) induced positive logD values, thereby rendering most of the respective complexes to be bioactive; 2) complexes with 2quinolyl substituted 1,2,3-triazole ligands (b) displayed better effects than those with 2-pyridyl substituents (a); 3) the compounds showed widespread activity among cancer cell lines; 4) cooperative binding of the complexes took place to their targets reflected by Hill coefficients larger than 1; 5) p-cym-Ru(II), p-cym-Os(II), and Cp*-Ir(III) complexes possessed bioactivity in contrast to Cp*-Rh(III) derivatives, and the p-cym-Os(II) complexes with the lowest IC50 values on cancer cells were the most efficient members of the set. Although complexes with slightly lower tendency for hydrolysis were detected in the organorhodium-3a system than in the organoruthenium system, as indicated by the solution equilibrium study, inactivity of Rh-3a can be explained by the rather labile character of this complex compared to those formed with the other three metal ions.

In terms of biological effects, the α -anomer-containing complexes (a-complexes hereafter) phenocopied certain features of the previously described β-anomer-containing complexes (Kacsir et al., 2021; Kacsir et al., 2022; Kacsir et al., 2023a) (βcomplexes hereafter) in terms of 1) selectivity toward cancer cells, 2) the induction of oxidative stress to induce cytostasis or bacteriostasis, and 3) effectiveness on cisplatin-resistant cells. On mammalian cells, the α -complexes had similar potency (i.e., similar IC_{50} values) as the β -complexes. Furthermore, the pattern of the IC_{50} values was also similar between the α - and β -complexes, with the lowest IC₅₀ values on A2780 and ID8 cells, somewhat higher IC₅₀ values on other cancer cell lines and an at least ten-fold larger IC50 on human primary dermal fibroblasts. The lowest IC₅₀ value among the complexes described in this report on A2780 cells is submicromolar (0.65 μM for Os-4b), with a corresponding IC₅₀ value on primary human dermal fibroblasts of 10.54 µM. The corresponding β-complex (Kacsir et al., 2023a) had an IC₅₀ value of 0.58 μM on A2780 cells, and the IC_{50} value was not detectable on primary human dermal fibroblasts.

Although the α- and β-complexes had similar behavior on mammalian cells, marked differences were observed with regard to their bacteriostatic capacity. Namely, the a-complexes with O-perbenzoylated glucose units were active only on a subset of the MRSA isolates and were largely inactive on VRE isolates. This was unexpected, as in previous studies, β -complexes with similar structural components were active on all of the MRSA and VRE isolates used in our current study (Balázs et al., 2022; Kacsir et al., 2023a; Kacsir et al., 2023b). Only one complex, Os-5a from the present study, was bacteriostatic on all MRSA and VRE isolates with low micromolar average MIC values (6.8 μM on MRSA and 5 μM on VRE isolates). Interestingly, bacteriostatic complexes had lower IC50 values on mammalian cells than their MIC values on bacteria. The MIC value of Os-5a is comparable to the MIC values of the previously identified bacteriostatic complexes (Balázs et al., 2022; Kacsir et al., 2023a; Kacsir et al., 2023b). Of note, a limitation of our study is the low number of clinical isolates.

There are literature reports for the antibacterial activity of piano stool complexes of ruthenium, rhodium, iridium, and osmium on

Mycobacterium species (Karpin et al., 2013; DuChane et al., 2018; Yufanyi et al., 2020; Bernier et al., 2021; Coverdale et al., 2021), Klebsiella pneumoniae, Escherichia coli, and S. aureus (Lapasam et al., 2020a; Lapasam et al., 2020c). The inhibitory properties of the complexes cannot be directly compared to our results in the case of each study as different model systems are used in certain reports (i.e., disc diffusion test versus MIC value determination), nevertheless, for the compatible studies, Os(II) complexes had comparable or superior MIC values on Mycobacterium ((Coverdale et al., 2021) 1.25-2.5 µM; (Bernier et al., 2021); best MIC value 0.45 μ M). Unfortunately, the inhibitory values for Staphylococcus aureus (Lapasam et al., 2020a; Lapasam et al., 2020c) are not comparable due to the aforementioned technical differences. Of note, a bacteriostatic property is not a common trait for the halfsandwich complexes with a similar structure to those assessed in this study (Pivarcsik et al., 2022) vs. (Balázs et al., 2022; Kacsir et al., 2023a; Kacsir et al., 2023b).

Taken together, the change of the configuration of the C1 carbon of the carbohydrate moiety from β to α did not largely affect the antineoplastic activity of the complexes. However, the $\alpha\text{-complexes}$ had limited bacteriostatic activity, and only the complex with pentanoyl protective groups on the carbohydrate moiety exerted bacteriostatic activity. Our study suggests that while similar structural components render half-sandwich complexes cytostatic and bacteriostatic, different structural modifications are necessary for bacteriostatic activity or cytostatic activity; hence, complexes must be fine-tuned as a function of the intended use.

4 Materials and Methods

4.1 Syntheses

4.1.1 General methods

Optical rotation measurements were conducted on a Jasco P-2000 polarimeter (Jasco, Easton, MD, USA) at ambient temperature, with reported values representing the average of three parallel determinations. NMR spectra were recorded using Bruker (Karlsruhe, Germany) spectrometers: DRX360 (360/ 90 MHz for ¹H/¹³C), DRX400 (400/100 MHz for ¹H/¹³C), and Avance II 500 (500/125 MHz for ¹H/¹³C). Me₄Si was applied as the reference for chemical shifts of ¹H-NMR, while the residual solvent signals were used for those of ¹³C-NMR. The proton- and carbon-signal assignments for characteristic resonances of the prepared complexes were based on COSY and HSQC correlations of some representatives of the series (Ru-2b, Ir-2b, Os-4b, Rh-**4b**). ESI-HRMS data were obtained by measurements on a Bruker maXis II spectrometer using positive ionization mode. TLC analyses were conducted on DC Kieselgel 60 F₂₅₄ plates (Sigma-Aldrich), with visualization achieved under UV light or by gentle heating. For purifications carried out by column chromatography, Kieselgel 60 silica gel (particle size 0.063-0.2 mm, Molar Chemicals) was used as the stationary phase. Among the anhydrous solvents used, pyridine was acquired from VWR Chemicals, while the others were prepared in our laboratory following established distillation protocols: halogenated solvents (CH2Cl2 and CHCl3) were distilled from P₄O₁₀ and stored over 4 Å molecular sieves, and

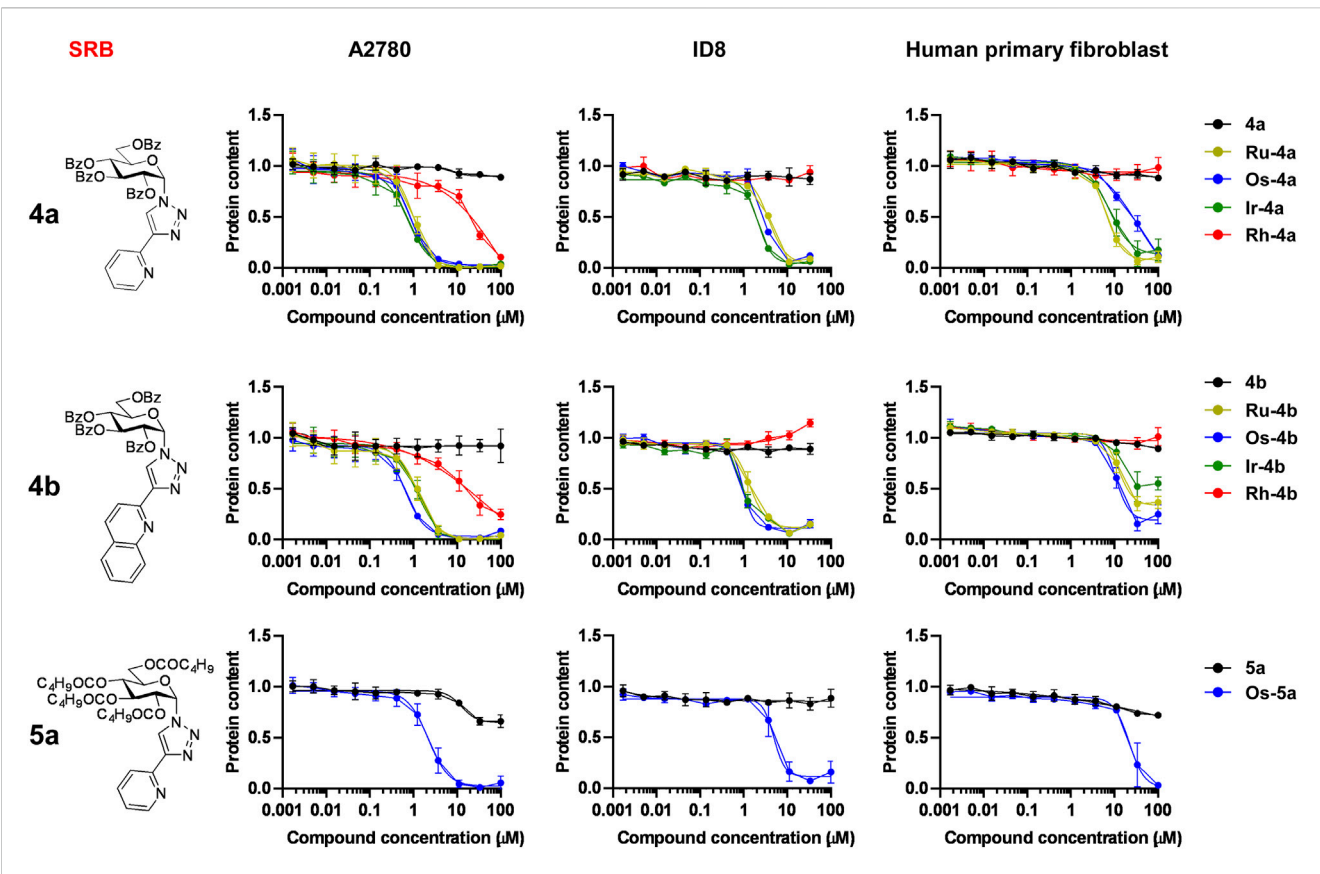


FIGURE 7
The ruthenium, somium, and iridium complexes of ligands $\bf 4a$, $\bf 4b$, and $\bf 5a$ are cytostatic on ovarian cancer models with a good therapeutic index. For SRB assays, 1.5×10^3 A2780 cells, 1.5×10^3 ID8 cells, or 4×10^3 primary fibroblasts were plated into 96-well plates. Cells were treated with the compounds in the concentrations indicated for 48 h. Data are represented as average \pm SD, from four biological replicates on A2780 and human primary fibroblasts, except in the case of Os complexes, where experiments were performed in three biological replicates. ID8 cells were assessed in three biological replicates. Individual assays were performed in duplicate. Values were normalized for vehicle-treated cells, and the absorbance for vehicle-treated cells equals 1. Normality was assessed using the D'Agostino-Pearson test. Statistical significance was assessed using a two-way ANOVA test followed by Tukey's post hoc test. For better visibility, normality, transformations, statistical tests, and p values are presented in an MS Excel sheet at https://figshare.com/s/3a0aa60b66f3f746f41e. Nonlinear regression was performed on the datasets; $|C_{50}|$ values are indicated in Table 5. Color code: black—free ligand (4a,b or 5a), khaki—ruthenium complex (Ru-4a,b), blue—osmium complex (Os-4a,b or Os-5a), green—iridium complex (Ir-4a,b), and red—rhodium complex (Rh-4a,b).

methanol was dried by distillation over magnesium turnings and iodine. 2-Ethynylpyridine (TCI Chemicals), pentanoyl chloride (Alfa Aesar), TlPF₆ (Strem Chemicals), dichloro (η^6 -p-cymene) ruthenium(II) dimer (**Ru-dimer**, Strem Chemicals), dichloro (η^5 -pentamethylcyclopentadienyl)iridium(III) dimer (**Ir-dimer**, Acros Organics), and dichloro (η^5 -pentamethylcyclopentadienyl) rhodium(III) dimer (**Rh-dimer**, Alfa Aesar) were purchased from the given suppliers. 2,3,4,6-Tetra-O-acetyl- α -D-glucopyranosyl azide (Zhang et al., 1999) (1), 2-ethynylquinoline (Son et al., 2013), and dichloro (η^6 -p-cymene)osmium(II) dimer (Godó et al., 2012) (**Os-dimer**) were synthesized in accordance with literature methods.

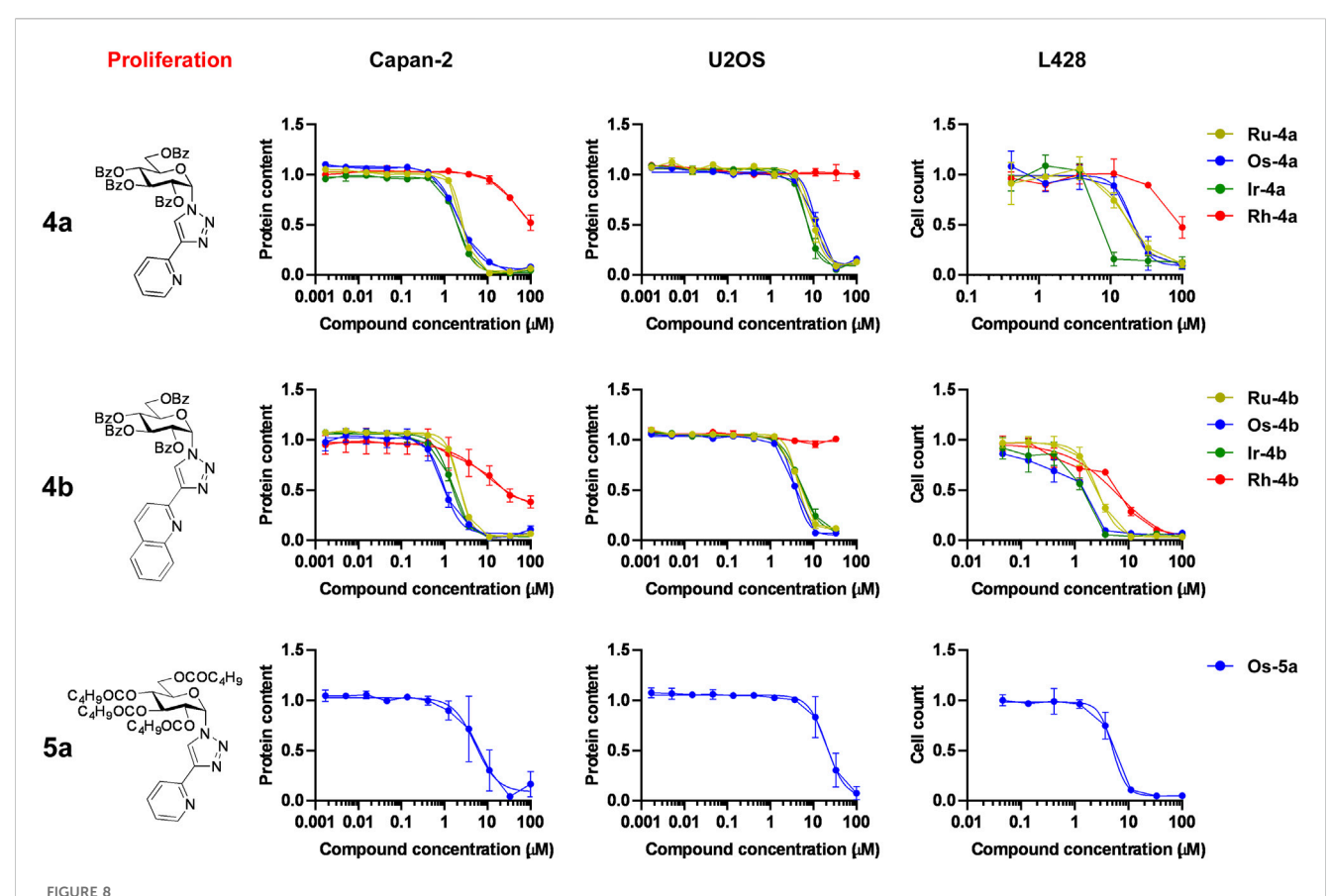
4.1.2 General procedure I for the synthesis of 1-(2',3',4',6'-tetra-O-acetyl- α -D-glucopyranosyl)-4-hetaryl-1,2,3-triazoles

2,3,4,6-Tetra-O-acetyl- α -D-glucopyranosyl azide (Zhang et al., 1999) (1) was dissolved in a solvent mixture of t-BuOH-H₂O (15–15 mL/1 g of azide). To this solution, the corresponding 2-ethynylated heterocycle (1.4 equiv.), L-ascorbic acid (0.8 equiv.) and CuSO₄·5H₂O (0.2 equiv.) were added. The reaction

mixture was heated at 70° C under stirring. When the TLC (1:1 EtOAchexane) showed complete disappearance of the starting azide (~1 day), the reaction mixture was diluted with water (30 mL) and extracted with CH₂Cl₂ (3 × 50 mL). The organic layers were combined and washed with 5% EDTA in 1 M aqueous solution of NH₄OH (30 mL), then with water (50 mL). The separated organic phase was dried over anhydrous MgSO₄, filtered, and evaporated under diminished pressure. Purification of the residual crude product was carried out by column chromatography.

4.1.3 General procedure II for the deacetylation of the 1-(2',3',4',6'-tetra-O-acetyl- α -D-glucopyranosyl)-4-hetaryl-1,2,3-triazoles by the Zemplén method

The appropriate O-peracetylated 1-(2',3',4',6'-tetra-O-acetyl- α -D-glucopyranosyl)-4-hetaryl-1,2,3-triazole (**2a,b**) was dissolved in a solvent mixture of anhydrous methanol and anhydrous chloroform (2–2 mL/100 mg of triazole). To this solution, a few drops of a 1 M solution of sodium methoxide in methanol were added to adjust the pH to a range of 8–9. The reaction mixture was left to stand at ambient temperature, and the transformation was monitored by



The complexes of ligands 4a, 4b, and 5a have cytostatic properties on a larger set of neoplasia cell models. For the assay, 1.5×10^3 Capan2, 4×10^3 U2OS, or 5×10^3 L428 cells were plated into 96-well plates. Capan2 and U2OS cells were treated with the compounds in the concentrations indicated for 4a h, and then an SRB assay was performed. L428 cells were treated with the compounds in the concentrations indicated for 9a h, and then an SRB assay was performed. L428 cells were treated with the compounds in the concentrations indicated for 9a h, and then the cells were counted using a Bürker chamber. Data are represented as average \pm SD from three biological replicates; individual assays were performed in duplicate. Values were normalized for vehicle-treated cells, and the absorbance for vehicle-treated cells equals 1. Normality was assessed using the Shapiro-Wilk test. Statistical significance was assessed using one-way ANOVA or Kruskal-Wallis test as a function of normality, followed by Holm-Sidak's, Dunnett's, or Dunn's post hoc test, respectively. For better visibility, normality, transformations, statistical tests, and p values are presented in an MS Excel sheet at https://figshare.com/s/3a0aa60b66f3f746f41e. Nonlinear regression was performed on the datasets; IC $_{50}$ values are indicated in Table 5. Color code: khaki-ruthenium complex (Ru-4a,b), blue—osmium complex (Os-4a,b or Os-5a), green—iridium complex (Ir-4a,b), and red—rhodium complex (Rh-4a,b).

TLC (1:1 EtOAc-hexane and 7:2 CHCl₃-MeOH). After completion of the reaction, the mixture was treated with a cation exchange resin (Amberlyst 15, in H⁺ form) for neutralization. Subsequently, the resin was removed by filtration, and the solution was concentrated under reduced pressure. The pure compound was obtained by column chromatographic purification.

4.1.4 General procedure III for the *O*-peracylation of the 1- $(\alpha$ -D-glucopyranosyl)-4-hetaryl-1,2,3-triazoles

The corresponding 1-(α -D-glucopyranosyl)-4-hetaryl-1,2,3-triazole (**3a,b**) was dissolved in anhydrous pyridine (4 mL/50 mg triazole). To this solution, the appropriate carboxylic acid chloride (4.8 equiv.) was added under stirring. The reaction mixture was subsequently heated to 60°C, and the transformation was monitored by TLC (7:2 CHCl₃-MeOH and 1:2 EtOAc-hexane). After 2 h, the TLC indicated incompleteness of the reaction; therefore, additional portions

of acid chloride (2 \times 4.8 equiv. per 4 h) were added to the mixture, and then the stirring was continued at 60°C overnight. After that, the pyridine was removed under reduced pressure, and the residue was diluted with water (20 mL) and extracted with CHCl₃ (2 \times 20 mL). The combined organic layers were extracted with a saturated aqueous solution of NaHCO₃ (3 \times 20 mL), then with water (20 mL). The organic layer was dried (MgSO₄), filtered, and the solvent was removed *in vacuo*. The target pure compound was obtained by column chromatographic purification of the residue.

4.1.5 General procedure IV for the synthesis of the half-sandwich platinum-group metal complexes of the O-peracylated and O-unprotected 1-(α -D-glucopyranosyl)-4-hetaryl-1,2,3-triazoles

To a solution of the appropriate dimeric chlorobridged metal complex (Ru-dimer/Os-dimer/Ir-dimer/Rh-dimer) in anhydrous CH_2Cl_2 (1 mL/10 mg dimer), the

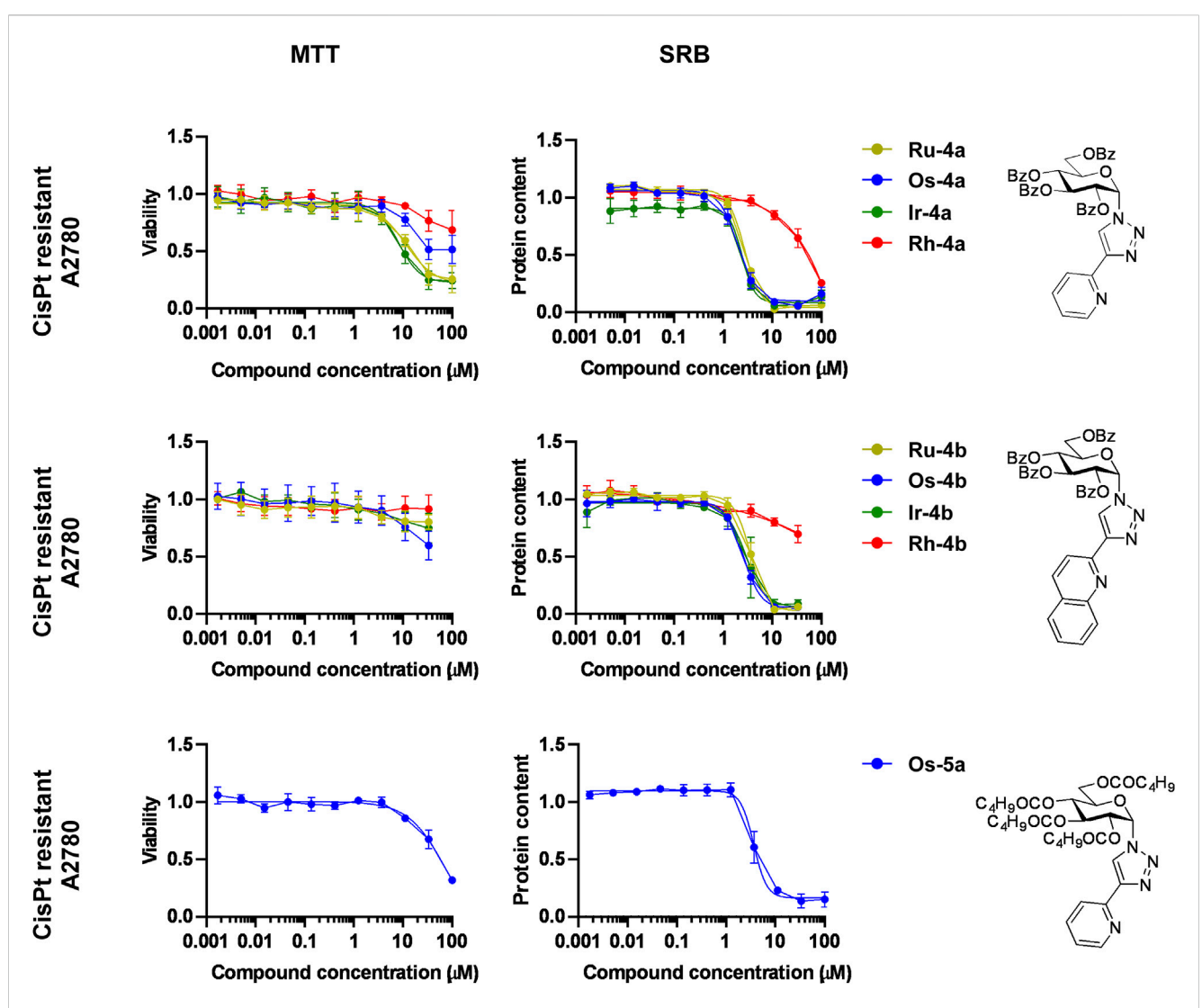


FIGURE 9
The complexes of ligands 4a, 4b, and 5a have cytostatic properties on cisplatin-resistant A2780 cells. For MTT assays, 6.5 × 10³ cisplatin-resistant A2780 cells were plated into 96-well plates, and for SRB assays, 4 × 10³ cisplatin-resistant A2780 cells were plated into 96-well plates. Cells were treated with the compounds in the concentrations indicated for either 4 h for an MTT assay or 48 h for an SRB assay. The n values for the assays are the following: n = 3 for Ru/Os-4a in SRB, Rh-4a, Ru/Ir-4b, and Os-5a in MTT and SRB; n = 4 for Ir-4a, Os/Rh-4b in MTT and SRB; n = 6 for Ru/Os-4a in MTT. Data are represented as average ± SD, and individual assays were performed in duplicate. Values were normalized for vehicle-treated cells, and the absorbance for vehicle-treated cells equals 1. Normality was assessed using the Shapiro-Wilk test. Statistical significance was assessed using one-way ANOVA or Kruskal-Wallis test as a function of normality, followed by Holm-Sidak's, Dunnett's, or Dunn's post hoc test. For better visibility, normality, transformations, statistical tests, and p values are presented in an MS Excel sheet at https://figshare.com/s/3a0aa60b66f3f746f41e. Nonlinear regression was performed on the datasets; IC₅₀ values are indicated in Table 5. Color code: khaki-ruthenium complex (Ru-4a,b), blue—osmium complex (Os-4a,b or Os-5a), green—iridium complex (Ir-4a,b), and red—rhodium complex (Rh-4a,b).

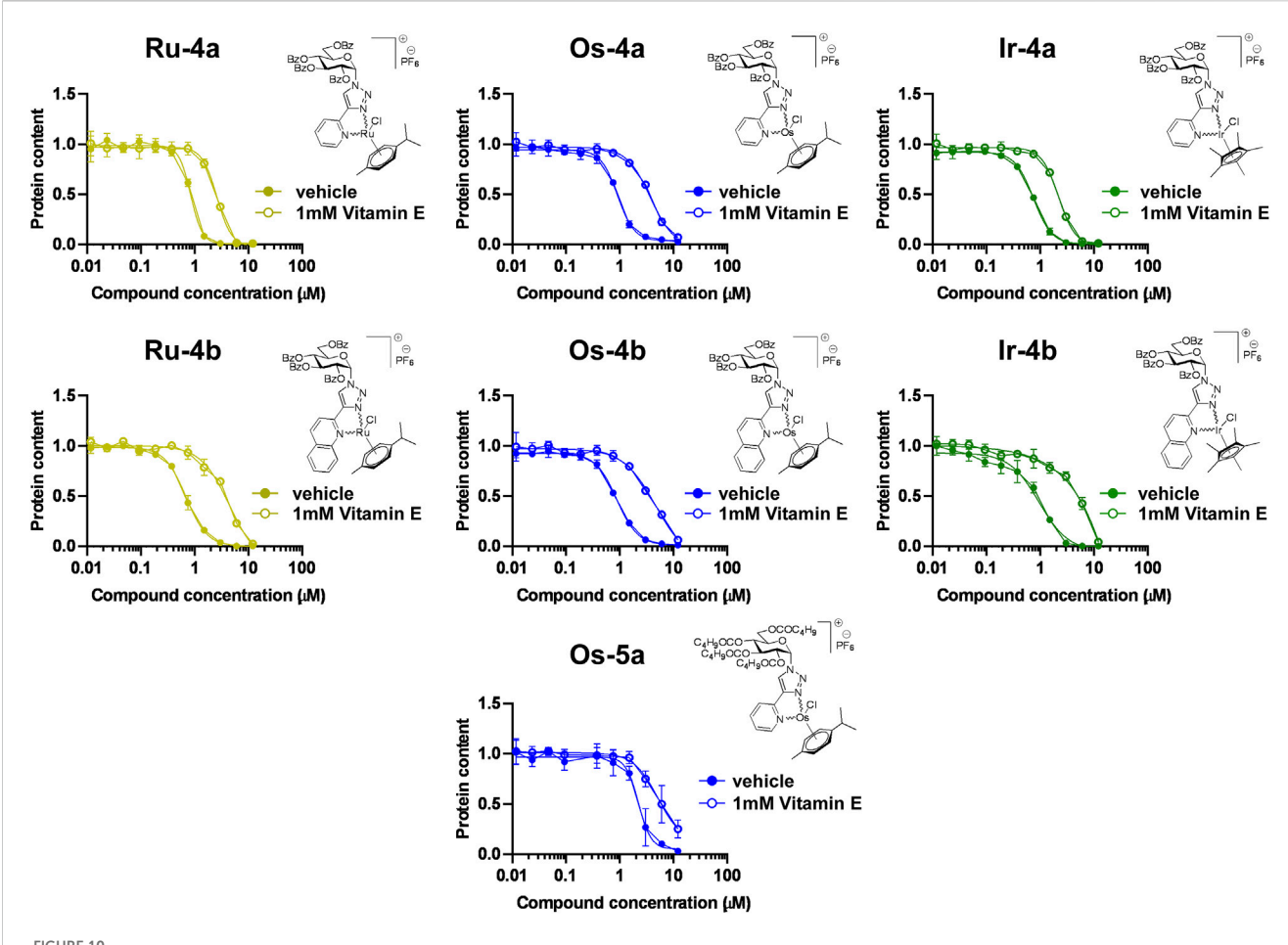
corresponding 1-(α -D-glucopyranosyl)-4-hetaryl-1,2,3-triazole (2.0–2.3 equiv.) and TlPF₆ (2 equiv.) were added. Under stirring at ambient temperature, anhydrous MeOH (1 mL/10 mg dimer) was also added to the reaction mixture to promote the precipitation of the TlCl. The stirring was continued at the same temperature until the TLC (95:5 CHCl₃-MeOH) indicated the total consumption of the dimer (\sim 1 h). The TlCl was removed by filtration using a syringe filter (Nylon, 25 mm, 0.22 µm), and the resulting solution was evaporated *in vacuo*. The pure complex from the residue was obtained by trituration in a solvent mixture, recrystallization, or column chromatographic purification.

4.2 Determination of the distribution coefficients (logD)

The distribution coefficient (logD) of the new complexes was determined using a 1:1 mixture of n-octanol-aq. PBS solution (pH = 7.4) according to our earlier published procedure (Kacsir et al., 2021).

4.3 Solution equilibrium studies

For solution studies, doubly deionized and ultra-filtered water was obtained from a Milli-Q RG (Millipore) water purification system.



The cytostatic effects of the complexes of ligands 4a, 4b, and 5a are alleviated by vitamin E. 1.5×10^3 A2780 cells were plated into 96-well plates. Cells were treated with the compounds in the concentrations indicated with or without vitamin E for 48 h, followed by an SRB assay. Data are represented as average \pm SD, from three biological replicates. Values were normalized for vehicle-treated cells, and the absorbance for vehicle-treated cells equals 1. Data are represented as fold change compared to vehicle-treated controls. Normality was assessed using the D'Agostino-Pearson test. Statistical significance was assessed using a two-way ANOVA test followed by Tukey's post hoc test. Nonlinear regression was performed on the datasets. For better visibility, normality, transformations, statistical tests, 10^{10} 0 values, and p values are presented in an MS Excel sheet at https://figshare.com/s/ 10^{10} 1 values are presented in an MS excel sheet at https://figshare.com/s/ 10^{10} 2 values and 10^{10} 3 values are presented in an MS excel sheet at https://figshare.com/s/ 10^{10} 3 values are presented in an MS excel sheet at https://figshare.com/s/ 10^{10} 3 values are presented in an MS excel sheet at https://figshare.com/s/ 10^{10} 3 values are presented in an MS excel sheet at https://figshare.com/s/ 10^{10} 3 values are presented in an MS excel sheet at https://figshare.com/s/ 10^{10} 3 values are presented in an MS excel sheet at https://figshare.com/s/ 10^{10} 3 values are presented in an MS excel sheet at https://figshare.com/s/ 10^{10} 3 values are presented cells, and the absorbance for 48 h, followed by Tukey in 50 h, but a series of 100 h, but a s

pH-potentiometric measurements were carried out at a constant ionic strength of 0.20 M KCl and at 25.0°C. Carbonate-free KOH solutions of known concentrations (ca. 0.2 M) were used as titrant. HCl stock solutions were prepared from concentrated HCl, respectively, and their concentrations were determined by potentiometric titrations using Gran's method (Gran et al., 1950). A Mettler Toledo DL50 titrator equipped with a DG114-SC combined glass electrode was used for the pH-potentiometric measurements. The electrode systems were calibrated according to Irving et al. (1967); the pHmetric readings could therefore be converted into hydrogen ion concentration. The water ionization constant, p K_w , was 13.74 ± 0.01 under the conditions employed. The initial volume of the samples was 15.00 mL. The metal ion concentrations were varied in the range 0.9-1.8 mM. The samples were in all cases completely deoxygenated by bubbling purified nitrogen for ca. 20 min before the measurements. The titrations were performed in the pH range of 2.0-11.0 in equilibrium-controlled mode, during which the pH equilibrium was assumed to be reached if a change in the measured potential was less than 0.1 mV within 90 s. The minimum waiting time was 1.5 min, while the maximum was up to 10 min. The protonation constants of the ligands and the overall stability constants of the complexes, $\beta_{p,q,r} = [M_p H_q L_r]/[M]^p [H]^q [L]^r$ (where "M" stands for $[(\eta^5 - Cp^*)Rh(H_2O)_3]^{2+}$ and "L" represents the completely deprotonated form of the ligand), were calculated with the aid of the SUPERQUAD (Gans et al., 1985) and PSEQUAD (Zékány and Nagypál, 1985) computer programs, respectively. During the calculations, hydrolysis of the metal ions was taken into consideration. The stability constants of the hydroxido complexes in chloride-containing medium involved in the equilibrium models were taken from the literature (Bíró et al., 2012; Bíró et al., 2013; Dömötör et al., 2014).

4.4 Chemicals for biology experiments

All chemicals used in the cell biology and biochemistry assays were obtained from Sigma-Aldrich unless otherwise stated. The free ligands and complexes investigated in this study were

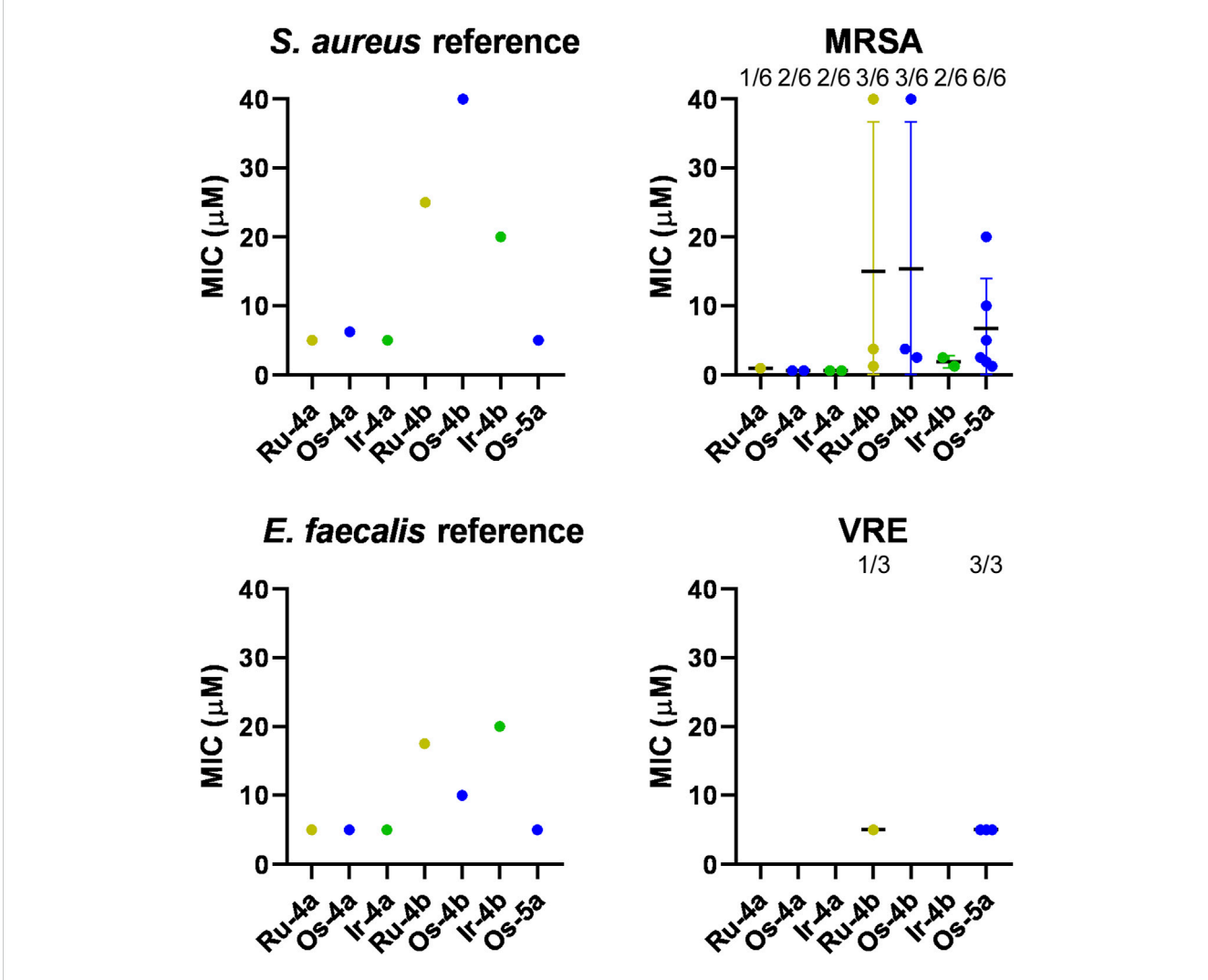


FIGURE 11
The bacteriostatic activity of the bioactive complexes on MRSA and VRE isolates. The MIC values of the complexes were determined against the reference strains of *S. aureus* (ATCC 29213) and *E. faecalis* (ATCC 29212) and clinical VRE and MRSA isolates by microdilution assays (repeated at least twice in duplicate) as described in Materials and Methods. The numbers indicate how many isolates were susceptible to the compound of those tested; that is, 1/6 indicates that one isolate was susceptible of six tested. Abbreviations: MRSA, methicillin-resistant *Staphylococcus aureus*; VRE, vancomycin-resistant *Enterococcus*. Color code: khaki—ruthenium complex (**Ru-4a,b**), blue—osmium complex (**Os-4a,b** or **Os-5a**), and green—iridium complex (**Ir-4a,b**).

dissolved in dimethyl sulfoxide for biology experiments, and 0.1% dimethyl sulfoxide was used as a vehicle control.

4.5 Cell culture

Cells were cultured under standard cell culture conditions: 37°C, 5% CO₂, humidified atmosphere. *A2780* cells were cultured in RPMI 1640 medium, supplemented with 10% fetal calf serum, 2 mM glutamine, and 1% penicillin–streptomycin.

ID8 cells were cultured in a high-glucose DMEM (4.5 g/L glucose) medium, supplemented with 4% fetal calf serum, 2 mM glutamine, 1% penicillin–streptomycin, and 1% ITS supplement (I3146).

 ${\it Capan2} \ {\it cells} \ {\it were} \ {\it maintained} \ {\it in} \ {\it MEM}, 10\% \ {\it fetal} \ {\it bovine} \ {\it serum}, 1\% \ {\it penicillin-streptomycin}, \ {\it and} \ 2 \ {\it mM} \ {\it glutamine}.$

Human primary dermal fibroblasts were cultured in low-glucose DMEM (1 g/L glucose) medium supplemented with 20% fetal calf serum, 2 mM glutamine, and 1% penicillin-streptomycin.

L428 cells were maintained in RPMI 1640 medium, supplemented with 10% fetal calf serum, 2 mM glutamine, and 1% penicillin–streptomycin.

U2OS cells were maintained in high-glucose DMEM (4.5 g/L glucose) medium, supplemented with 10% fetal calf serum, 2 mM glutamine, and 1% penicillin–streptomycin.

4.6 Bacterial reference strains

The reference strains of *Staphylococcus aureus* (ATCC 29213) and *Enterococcus faecalis* (ATCC 29212) were purchased from the ATCC (Manassas, VA, United States).

TABLE 6 The clinical isolates used in the study and the respective MIC values of the complexes on those isolates. Abbreviations: VRE—vancomycin-resistant Enterococcus, MRSA—methicillin-resistant Staphylococcus aureus.

Species and	Identifier	Sample	Year	MIC (μM)							
Strain				Ru- 4a	Os- 4a	Ir- 4a	Os- 4b	Ir- 4b	Ru- 4b	Os- 5a	
Reference E. faecalis				5	5	5	10	20	17.5	5	
VRE	25,051	Nephrostoma	2018	>40	>40	>40	>40	>40	>40	5	
	27,085	Wound	2018	>40	>40	>40	>40	>40	5	5	
	25,498	Rectal swab to screen for multiresistant pathogens	2018	>40	>40	>40	>40	>40	>40	5	
Reference S. aureus				5	6.25	5	40	20	25	5	
MRSA	24,272	Throat	2018	0.938	0.625	0.625	2.5	2.5	1.25	1.88	
	24,408	Bronchial	2018	>40	>40	>40	40	>40	40	2.5	
	20,426	Blood	2020	>40	>40	>40	>40	>40	>40	5	
	24,035	Wound	2018	>40	>40	>40	>40	>40	>40	1.25	
	24,328	Throat	2018	>40	0.625	0.625	3.75	1.25	3.75	20	
	24,268	Throat	2018	>40	>40	>40	>40	>40	>40	10	

4.7 Clinical isolates of *S. aureus* and *E. faecium*

We used a set of clinical isolates of *S. aureus* and *E. faecium* that were collected at the Medical Center of the University of Debrecen (Hungary) between 1 January 2018 and 31 December 2020. The isolates were reported in Balázs et al. (2022) and are presented in Table 6. The clinical isolates were identified using a Microflex MALDI-TOF mass spectrometer (Bruker, Billerica, MA, United States). The antibiotic susceptibility of the isolates was tested following the European Committee on Antimicrobial Susceptibility Testing (EUCAST) guidelines, which were valid at the time of collection.

4.8 Broth microdilution

Microdilution experiments were performed according to the standards of EUCAST (EUCAST, 2025). The bacterial isolates to be tested were grown on Mueller–Hinton agar plates. The inoculum density of bacteria was set at 5.0 \times 10 5 CFU/mL in microtiter plates in a final volume of 200 μL Mueller–Hinton broth. The tested concentration range was 0.08–40 μM (10 concentrations, two-fold serial dilutions), and a drug-free growth control and an inoculum-free negative control were included. The inoculated plates were incubated for 24 h at 37 $^{\circ}$ C, then visually assessed. Minimum inhibitory concentration (MIC) was defined as the lowest concentration with inhibitory effect compared to the growth control. All experiments were performed at least twice in duplicate.

4.9 Methylthiazolyldiphenyl-tetrazolium bromide (MTT) reduction assay

An MTT reduction assay measures the activity of mitochondrial complex I and can be used to detect toxicity (Henslee et al., 2016). The assay was performed in a manner similar to that described by Kacsir et al. (2023b). Briefly, cells were plated into 96-well plates the day before the assay. Cells were treated with the compounds for 4 h; then, MTT was added to a 0.5 mg/mL final concentration, and cells were incubated at 37°C in a cell incubator for 40-60 min, as a function of the cell line being assessed. The culture medium was removed, the reduced MTT dye was dissolved in dimethylsulfoxide, and plates were measured in a plate photometer (Thermo Scientific Multiscan GO spectrophotometer, Waltham, MA, United States) at 540 nm. Certain wells were designated to contain vehicle-treated cells on each plate. In calculations, the readings for these wells were considered to 1, and all readings were expressed relative to these values.

4.10 Sulforhodamine B (SRB) binding assay

An SRB assay measures protein content of cells in correlation with the cell number in an assay well and can therefore be used to assess cell proliferation or long-term cytostasis (Skehan et al., 1990). Cells were seeded into 96-well plates the day before the treatment for the assay. Cells were treated with the various compounds for 48 h. Then, the medium was removed, and cells were fixed with 10% trichloroacetic acid. Fixed cells were washed in distilled water three times, followed by staining with SRB (0.4 m/V%

dissolved in 1% acetic acid) for 10 min. Stained cells were washed in 1% acetic acid five times; the acetic acid was removed, and the cells were left to dry. Protein-bound SRB was released by adding 100 μL of 10 mM Tris base. Plates were measured in a plate photometer (Thermo Scientific Multiscan GO spectrophotometer, Waltham, MA, United States) at 540 nm. Certain wells were designated to contain vehicle-treated cells on each plate. In calculations, the readings for these wells were considered to be 1, and all readings were expressed relative to these values.

4.11 Annexin V-propidium iodide staining for the determination of cell death

The proportion of dead cells was assessed using the annexin V-propidium iodide assay and was measured using flow cytometry with an ACEA NovoCyte 3000 Flow Cytometer (Agilent Technologies, Santa Clara, CA, United States) instrument and the FITC annexin V/Dead Cell Apoptosis kit (Life Technologies, Eugene, OR, USA), according to the manufacturer's instructions, in a process similar to that described by Bai et al. (2001). Quadrants were set based on the FITC and propidium iodide (PI) values observed for the vehicle-treated cells. Double negative cells were considered living cells, and the other three quadrants were considered cells in different modes and phases of cell death and were added up. Heat-shocked cells were used as positive controls (30 min at 42°C in Eppendorf tubes similar to Nagy et al. (2007).

4.12 Statistical evaluation

Statistical analysis was performed using version 8.0.1 of GraphPad Prism. Values were tested for normal distribution using the D'Agostino-Pearson or Shapiro-Wilk normality tests. When necessary, values were log-normalized or normalized using the Box-Cox or two-step normalization method (Box and Cox, 1964), as indicated in the MS Excel file listing the values at https://figshare.com/s/3a0aa60b66f3f746f41e. The following statistical test, post hoc test, and the level of significance are indicated in the MS Excel file listing the values https://figshare.com/s/3a0aa60b66f3f746f41e. Nonlinear regression was performed using the built-in "[Inhibitor] vs response—Variable slope (four parameters), least square fit" utility of GraphPad, which yielded IC50 and Hill slope values if the sigmoid curves reached a plateau of inhibition, and there was no decrease between two subsequent data points or when inhibition was over 90%. In other cases, the percentage of inhibition was taken for the maximum concentration (100 µM).

Data availability statement

The datasets presented in the study can be found here: https://figshare.com/s/3a0aa60b66f3f746f41e.

Author contributions

AIZ: formal analysis, writing - original draft, writing - review and editing, and investigation. AS: Writing - original draft, Funding acquisition, Supervision, Writing - review and editing, Formal analysis, Data curation, Investigation, Visualization, Methodology, Validation, Conceptualization, and Project administration. IK: Validation, Data curation, Investigation, Writing - review and editing, and Writing - original draft. NIK: Writing - review and editing, Writing - original draft, Investigation. ÉK: Investigation, Writing - review and editing, and Writing - original draft. ES: Writing - original draft, Writing - review and editing, and Investigation. CF: Writing - original draft, Investigation, Validation, Supervision, Writing - review and editing, Methodology, and Project administration. MD: Methodology, Investigation, Writing - review and editing, and Writing - original draft. IR: Writing - original draft, Writing - review and editing, and Investigation. PBu: Supervision, Data curation, Writing - review and editing, Conceptualization, Methodology, Validation, Writing - original draft, Funding acquisition, and Project administration. AB: Visualization, Formal analysis, Investigation, Writing - review and editing, and Writing - original draft. EAJ: Data curation, Validation, Writing - original draft, Writing - review and editing, and Supervision. GK: Conceptualization, Validation, Writing - review and editing, Supervision, and Writing - original draft. LS: Funding acquisition, Supervision, Writing - review and editing, Conceptualization, and Writing - original draft. PBa: Supervision, Writing - review and editing, Conceptualization, Visualization, Validation, Writing - original draft, Project administration, and Funding acquisition. ÉB: Visualization, Conceptualization, Project administration, Validation, Supervision, Writing - original draft, Writing - review and editing, and Data curation.

Funding

The author(s) declare that financial support was received for the research and/or publication of this article. This project was funded by the National Research, Development and Innovation Office of Hungary (grants K142141, FK146852, K146147, K146656, TKP2021-EGA-19, and TKP2021-EGA-20). AS was supported by the Bolyai fellowship. Project no. TKP2021-EGA-19 and TKP2021-EGA-20 have been implemented with the support provided by the National Research, Development and Innovation Fund of Hungary, financed under the TKP2021-EGA funding scheme. Supported by the University of Debrecen Scientific Research Bridging Fund (DETKA). Supported by the University of Debrecen Program for Scientific Publication. AIZ was supported by the Stipendium Hungaricum Scholarship application no. 424368 and by the Missions Department of the Egyptian Ministry of Higher Education and Scientific Research/Vienna office.

Acknowledgments

The authors are grateful for the technical assistance from Kitti Barta and György Attila Kiss.

Conflict of interest

The authors declare that the research was conducted in the absence of any commercial or financial relationships that could be construed as a potential conflict of interest.

The author(s) declared that they were an editorial board member of Frontiers, at the time of submission. This had no impact on the peer review process and the final decision.

Generative AI statement

The author(s) declare that no Generative AI was used in the creation of this manuscript.

References

Bai, P., Bakondi, E., Szabó, E., Gergely, P., Szabó, C., and Virág, L. (2001). Partial protection by poly(ADP-ribose) polymerase inhibitors from nitroxyl-induced cytotoxity in thymocytes. *Free Radic. Biol. Med.* 31, 1616–1623. doi:10.1016/s0891-5849(01)00756-0

Bakewell, S., Conde, I., Fallah, Y., McCoy, M., Jin, L., and Shajahan-Haq, A. N. (2020). Inhibition of DNA repair pathways and induction of ROS are potential mechanisms of action of the small molecule inhibitor BOLD-100 in breast cancer. *Cancers* 12, 2647. doi:10.3390/cancers12092647

Balázs, B., Tóth, Z., Kacsir, I., Sipos, A., Buglyó, P., Somsák, L., et al. (2022). Targeting multiresistant Gram-positive bacteria by ruthenium, osmium, iridium and rhodium half-sandwich type complexes with bidentate monosaccharide ligands. Front. Chem. 10, 868234. doi:10.3389/fchem.2022.868234

Bashir, M., Mantoo, I. A., Arjmand, F., Tabassum, S., and Yousuf, I. (2023). An overview of advancement of organoruthenium(II) complexes as prospective anticancer agents. *Coord. Chem. Rev.* 487, 215169. doi:10.1016/j.ccr.2023.215169

Bernier, C. M., DuChane, C. M., Martinez, J. S., Falkinham, J. O., and Merola, J. S. (2021). Synthesis, characterization, and antimicrobial activity of Rh^{III} and Ir^{III} N-heterocyclic carbene piano-stool complexes. *Organometallics* 40, 1670–1681. doi:10.1021/acs.organomet.1c00166

Bíró, L., Farkas, E., and Buglyó, P. (2012). Hydrolytic behaviour and chloride ion binding capability of $[Ru(\eta^6\text{-}p\text{-}cym)(H_2O)_3]^{2^+}$: a solution equilibrium study. *Dalton Trans.* 41, 285–291. doi:10.1039/C1DT11405K

Bíró, L., Godó, A. J., Bihari, Z., Garribba, E., and Buglyó, P. (2013). Tuning the hydrolytic properties of half-sandwich-type organometallic cations in aqueous solution. *Eur. J. Inorg. Chem.* 2013, 3090–3100. doi:10.1002/ejic.201201527

Boros, E., Dyson, P. J., and Gasser, G. (2020). Classification of metal-based drugs according to their mechanisms of action. *Chem.* 6, 41–60. doi:10.1016/j.chempr.2019.10.013

Bortolamiol, E., Visentin, F., and Scattolin, T. (2023). Recent advances in bioconjugated transition metal complexes for cancer therapy. *Appl. Sci.* 13, 5561. doi:10.3390/app13095561

Box, G. E. P., and Cox, D. R. (1964). An analysis of transformations. *J. R. Stat. Soc.* 26, 211–243. doi:10.1111/j.2517-6161.1964.tb00553.x

Burris, H. A., Bakewell, S., Bendell, J. C., Infante, J., Jones, S. F., Spigel, D. R., et al. (2016). Safety and activity of IT-139, a ruthenium-based compound, in patients with advanced solid tumours: a first-in-human, open-label, dose-escalation phase I study with expansion cohort. ESMO. Open 1, e000154. doi:10.1136/esmoopen-2016-000154

Chmurzyński, L. (2000). The basicity of pyridine and its tendency towards cationic homoconjugation in non-aqueous media. *J. Het. Chem.* 37, 71–74. doi:10.1002/jhet. 5570370111

Chuong, C., DuChane, C. M., Webb, E. M., Rai, P., Marano, J. M., Bernier, C. M., et al. (2021). Noble metal organometallic complexes display antiviral activity against SARS-CoV-2. *Viruses* 13, 980. doi:10.3390/v13060980

Coverdale, J. P. C., Guy, C. S., Bridgewater, H. E., Needham, R. J., Fullam, E., and Sadler, P. J. (2021). Osmium-arene complexes with high potency towards *Mycobacterium tuberculosis. Metallomics* 13, mfab007. doi:10.1093/mtomcs/mfab007

Coverdale, J. P. C., Laroiya-McCarron, T., and Romero-Canelón, I. (2019). Designing ruthenium anticancer drugs: what have we learnt from the key drug candidates? *Inorganics* 7, 31. doi:10.3390/inorganics7030031

Desiatkina, O., Paunescu, E., Mösching, M., Anghel, N., Boubaker, G., Amdouni, Y., et al. (2020). Coumarin-tagged dinuclear trithiolato-bridged ruthenium(II) arene complexes: photophysical properties and antiparasitic activity. *ChemBioChem* 21, 2818–2835. doi:10.1002/cbic.202000174

Publisher's note

All claims expressed in this article are solely those of the authors and do not necessarily represent those of their affiliated organizations, or those of the publisher, the editors and the reviewers. Any product that may be evaluated in this article, or claim that may be made by its manufacturer, is not guaranteed or endorsed by the publisher.

Supplementary material

The Supplementary Material for this article can be found online at: https://www.frontiersin.org/articles/10.3389/fchem.2025.1619991/full#supplementary-material

Dimitrijevic, M. V., Mihajlovic-Lalic, L. E., Grguric-Sipka, S., Mihajlov-Krstev, T. M., Miladinovic, D. L., and Poljarevic, J. M. (2023). Synthesis, chemical characterization, and antimicrobial potency of picolinate-based half-sandwich Ru(II) complexes. *J. Coord. Chem.* 76, 783–797. doi:10.1080/00958972.2023.2195965

Dömötör, O., Aicher, S., Schmidlehner, M., Novak, M. S., Roller, A., Jakupec, M. A., et al. (2014). Antitumor pentamethylcyclopentadienyl rhodium complexes of maltol and allomaltol: synthesis, solution speciation and bioactivity. *J. Inorg. Biochem.* 134, 57–65. doi:10.1016/j.jinorgbio.2014.01.020

DuChane, C. M., Brown, L. C., Dozier, V. S., and Merola, J. S. (2018). Synthesis, characterization, and antimicrobial activity of Rh^{III} and Ir^{III} β -diketonato piano-stool compounds. $\textit{Organometallics}\ 37,\ 530–538.$ doi:10.1021/acs.organomet.7b00742

EUCAST (2025). MIC determination of non-fastidious and fastidious organisms. EUCAST. Available online at: https://www.eucast.org/ast_of_bacteria/mic_determination/?no_cache=1 (Accessed November 4, 2021).

Fandzloch, M., Jedrzejewski, T., Dobrzanska, L., Esteban-Parra, G. M., Wisniewska, J., Paneth, A., et al. (2021). New organometallic ruthenium(II) complexes with purine analogs - a wide perspective on their biological application. *Dalton Trans.* 50, 5557–5573. doi:10.1039/d0dt03974h

Fernandes, A. C. (2019). Synthesis, biological activity and medicinal applications of ruthenium complexes containing carbohydrate ligands. *Curr. Med. Chem.* 26, 6412–6437. doi:10.2174/0929867326666190124124350

Gambino, D. (2024). Organometallics in medicinal chemistry: antiparasitic agents. J. Braz. Chem. Soc. 35. e-20240104. doi:10.21577/0103-5053.20240104

Gano, L., Pinheiro, T., Matos, A. P., Tortosa, F., Jorge, T. F., Gonçalves, M. S., et al. (2019). Antitumour and toxicity evaluation of a Ru(II)-Cyclopentadienyl complex in a prostate cancer model by imaging tools. *Anti-Cancer Agents Med. Chem.* 19, 1262–1275. doi:10.2174/1871520619666190318152726

Gans, P., Sabatini, A., and Vacca, A. (1985). SUPERQUAD: an improved general program for computation of formation constants from potentiometric data. *J. Chem. Soc. Dalton Trans.*, 1195–1200. doi:10.1039/dt9850001195

Gichumbi, J. M., and Friedrich, H. B. (2018). Half-sandwich complexes of platinum group metals (Ir, Rh, Ru and Os) and some recent biological and catalytic applications. *J. Organomet. Chem.* 866, 123–143. doi:10.1016/j. jorganchem.2018.04.021

Godó, A. J., Bényei, A. C., Duff, B., Egan, D. A., and Buglyó, P. (2012). Synthesis and X-ray diffraction structures of novel half-sandwich Os(II)- and Ru(II)-hydroxamate complexes. RSC Adv. 2, 1486–1495. doi:10.1039/C1RA00998B

Gombos, I., Crul, T., Piotto, S., Güngör, B., Török, Z., Balogh, G., et al. (2011). Membrane-lipid therapy in operation: the HSP co-inducer BGP-15 activates stress signal transduction pathways by remodeling plasma membrane rafts. *PLoS One* 6, e28818. doi:10.1371/journal.pone.0028818

Gran, G., Dahlenborg, H., Laurell, S., and Rottenberg, M. (1950). Determination of the equivalent point in potentiometric titrations. *Acta Chem. Scand.* 4, 559–577. doi:10. 3891/acta.chem.scand.04-0559

Hanif, M., Babak, M. V., and Hartinger, C. G. (2014). Development of anticancer agents: wizardry with osmium. *Drug Discov. Today* 19, 1640–1648. doi:10.1016/j.drudis. 2014.06.016

Hartinger, C. G., Phillips, A. D., and Nazarov, A. A. (2011). Polynuclear ruthenium, osmium and gold complexes. The quest for innovative anticancer chemotherapeutics. *Curr. Top. Med. Chem.* 11, 2688–2702. doi:10.2174/156802611798040769

- Hartmann, J. T., and Lipp, H.-P. (2003). Toxicity of platinum compounds. *Expert Opin. Pharmacother.* 4, 889–901. doi:10.1517/14656566.4.6.889
- Henslee, E. A., Torcal Serrano, R. M., Labeed, F. H., Jabr, R. I., Fry, C. H., Hughes, M. P., et al. (2016). Accurate quantification of apoptosis progression and toxicity using a dielectrophoretic approach. *Analyst* 141, 6408–6415. doi:10.1039/c6an01596d
- Herić, A., Dibranin, N., Martić, L., Hodžić, E., Zahirović, A., and Kozarić, A. K. (2024). Ruthenium-based complexes as anti-tumor agents. *J. Health Sci.* 14, 70–83. doi:10.17532/jhsci.2024.2693
- Holzer, I., Desiatkina, O., Anghel, N., Johns, S. K., Boubaker, G., Hemphill, A., et al. (2022). Trithiolato-bridged dinuclear arene ruthenium(II)-glycoconjugates: synthesis and antiparasitic activity. *ChemRxiv Camb. Camb. Open Engag.* doi:10.26434/chemrxiv-2022-kkth
- Hon-Wing, L., Vang, M. J., and Mavis, R. D. (1981). The cooperative interaction between vitamin E and vitamin C in suppression of peroxidation of membrane phospholipids. *Biochim. Biophys. Acta, Lipids Lipid. Metab.* 664, 266–272. doi:10.1016/0005-2760(81)90049-7
- Horváth, I., Glatz, A., Varvasovszki, V., Török, Z., Páli, T., Balogh, G., et al. (1998). Membrane physical state controls the signaling mechanism of the heat shock response in Synechocystis PCC 6803: identification of hsp17 as a "fluidity gene". *Proc. Nat. Acad. Sci. U. S. A.* 95, 3513–3518. doi:10.1073/pnas.95.7.3513
- Irving, H., Miles, M., and Pettit, L. (1967). A study of some problems in determining the stoicheiometric proton dissociation constants of complexes by potentiometric titrations using a glass electrode. *Anal. Chim. Acta* 38, 475–488. doi:10.1016/S0003-2670(01)80616-4
- Jankovic, N., Milovic, E., Jovanovic, J. D., Markovic, Z., Vranes, M., Stanojkovic, T., et al. (2022). A new class of half-sandwich ruthenium complexes containing Biginelli hybrids: anticancer and anti-SARS-CoV-2 activities. *Chem. Biol. Interact.* 363, 110025. doi:10.1016/j.cbi.2022.110025
- Kacsir, I., Sipos, A., Bényei, A., Janka, E., Buglyó, P., Somsák, L., et al. (2022). Reactive oxygen species production is responsible for antineoplastic activity of osmium, ruthenium, iridium and rhodium half-sandwich type complexes with bidentate glycosyl hetero-cyclic ligands in various cancer cell models. *Int. J. Mol. Sci.* 23, 813. doi:10.3390/jims23020813
- Kacsir, I., Sipos, A., Kiss, T., Major, E., Bajusz, N., Tóth, E., et al. (2023a). Half sandwich-type osmium, ruthenium, iridium and rhodium complexes with bidentate glycosyl heterocyclic ligands induce cytostasis in platinum-resistant ovarian cancer cells and bacteriostasis in gram-positive multiresistant bacteria. *Front. Chem.* 11, 1086267. doi:10.3389/fchem.2023.1086267
- Kacsir, I., Sipos, A., Major, E., Bajusz, N., Bényei, A., Buglyó, P., et al. (2023b). Half-sandwich type platinum-group metal complexes of *C*-glucosaminyl azines: synthesis and antimeoplastic and antimicrobial activities. *Molecules* 28, 3058. doi:10.3390/molecules28073058
- Kacsir, I., Sipos, A., Ujlaki, G., Buglyó, P., Somsák, L., Bai, P., et al. (2021). Ruthenium half-sandwich type complexes with bidentate monosaccharide ligands show antineoplastic activity in ovarian cancer cell models through reactive oxygen species production. *Int. J. Mol. Sci.* 22, 10454. doi:10.3390/ijms221910454
- Karpin, G. W., Merola, J. S., and Falkinham, J. O. (2013). Transition metal-α-amino acid complexes with antibiotic activity against *Mycobacterium* spp. *Antimicrob. Agents Chemother.* 57, 3434–3436. doi:10.1128/aac.00452-13
- Kenny, R. G., and Marmion, C. J. (2019). Toward multi-targeted platinum and ruthenium drugs-A new paradigm in cancer drug treatment regimens? *Chem. Rev.* 119, 1058–1137. doi:10.1021/acs.chemrev.8b00271
- Klaimanee, E., Nhukeaw, T., Saithong, S., Ratanaphan, A., Phongpaichit, S., Tantirungrotechai, Y., et al. (2021). Half-sandwich ruthenium (II) *p*-cymene complexes based on organophosphorus ligands: structure determination, computational investigation, *in vitro* antiproliferative effect in breast cancer cells and antimicrobial activity. *Polyhedron* 204, 115244. doi:10.1016/j.poly.2021.115244
- Kljun, J., Leon, I. E., Persic, S., Cadavid-Vargas, J. F., Etcheverry, S. B., He, W. J., et al. (2018). Synthesis and biological characterization of organoruthenium complexes with 8-hydroxyquinolines. *J. Inorg. Biochem.* 186, 187–196. doi:10.1016/j.jinorgbio.2018.
- Kljun, J., Scott, A. J., Rizner, T. L., Keiser, J., and Turel, I. (2014). Synthesis and biological evaluation of organoruthenium complexes with azole antifungal agents. First crystal structure of a tioconazole metal complex. *Organometallics* 33, 1594–1601. doi:10.1021/om401096y
- Konkankit, C. C., Marker, S. C., Knopf, K. M., and Wilson, J. J. (2018). Anticancer activity of complexes of the third row transition metals, rhenium, osmium, and iridium. *Dalton Trans.* 47, 9934–9974. doi:10.1039/c8dt01858h
- Koziel, S., Wojtala, D., Szmitka, M., Lesiow, M., Ziolkowska, A., Sawka, J., et al. (2025). Half-sandwich organometallic Ir(III) and Ru(II) compounds and their interactions with biomolecules. *ChemPlusChem* 90, e202400621. doi:10.1002/cplu.202400621
- Kraft, J., Schmollinger, D., Maudrich, J., and Ziegler, T. (2015). Synthesis of sugarderived triazole-and pyridine-based metal complex ligands. *Synthesis* 47, 199–208. doi:10.1055/s-0034-1379473
- Kulkarni, G. S., Lilge, L., Nesbitt, M., Dumoulin-White, R. J., Mandel, A., and Jewett, M. A. S. (2022). A phase 1b clinical study of intravesical photodynamic therapy in

- patients with Bacillus calmette-guérin-unresponsive non-muscle-invasive bladder cancer. Eur. Urol. Open Sci. 41, 105–111. doi:10.1016/j.euros.2022.04.015
- Lapasam, A., Adhikari, S., Banothu, V., Addepally, U., and Kollipara, M. R. (2020a). Arene platinum group metal complexes containing imino-quinolyl ligands: synthesis and antibacterial studies. *J. Coord. Chem.* 73, 737–753. doi:10.1080/00958972.2020. 1753037
- Lapasam, A., Banothu, V., Addepally, U., and Kollipara, M. R. (2020b). Half-sandwich arene ruthenium, rhodium and iridium thiosemicarbazone complexes: synthesis, characterization and biological evaluation. *J. Chem. Sci.* 132, 34. doi:10.1007/s12039-019-1731-5
- Lapasam, A., Mawnai, I. L., Banothu, V., Kaminsky, W., and Kollipara, M. R. (2020c). Ruthenium, rhodium and iridium complexes containing pyrimidine based thienyl pyrazoles: synthesis and antibacterial studies. *J. Organomet. Chem.* 911, 121155. doi:10.1016/j.jorganchem.2020.121155
- Leijen, S., Burgers, S. A., Baas, P., Pluim, D., Tibben, M., van Werkhoven, E., et al. (2015). Phase I/II study with ruthenium compound NAMI-A and gemcitabine in patients with non-small cell lung cancer after first line therapy. *Investig. New Drugs* 33, 201–214. doi:10.1007/s10637-014-0179-1
- Leung, C. H., Zhong, H. J., Chan, D. S. H., and Ma, D. L. (2013). Bioactive iridium and rhodium complexes as therapeutic agents. *Coord. Chem. Rev.* 257, 1764–1776. doi:10. 1016/j.ccr.2013.01.034
- Li, Y., Liu, B., Shi, H., Wang, Y., Sun, Q., and Zhang, Q. (2021). Metal complexes against breast cancer stem cells. *Dalton Trans.* 50, 14498–14512. doi:10.1039/d1dt02909f
- Liu, J., Lai, H., Xiong, Z., Chen, B., and Chen, T. (2019). Functionalization and cancertargeting design of ruthenium complexes for precise cancer therapy. *Chem. Commun.* 55, 9904–9914. doi:10.1039/c9c04098f
- Liu, Z., and Sadler, P. J. (2014). Organoiridium complexes: anticancer agents and catalysts. Acc. Chem. Res. 47, 1174–1185. doi:10.1021/ar400266c
- Máliková, K., Masaryk, L., and Štarha, P. (2021). Anticancer half-sandwich rhodium(III) complexes. *Inorganics* 9, 26. doi:10.3390/inorganics9040026
- Mansour, A. M., Arafa, M. M., Hegazy, Y. S., Sadek, M. S., Ibrahim, H. H., Abdullah, Y. S., et al. (2025). A comprehensive survey of cytotoxic active half-sandwich Ir(III) complexes: structural perspective, and mechanism of action. *Dalton Trans.* 54, 4788–4847. doi:10.1039/d4dt03219e
- Martínez, A., Carreon, T., Iniguez, E., Anzellotti, A., Sánchez, A., Tyan, M., et al. (2012). Searching for new chemotherapies for tropical diseases: ruthenium-clotrimazole complexes display high *in vitro* activity against leishmania major and trypanosoma cruzi and low toxicity toward normal mammalian cells. *J. Med. Chem.* 55, 3867–3877. doi:10.1021/im300070h
- Mbaba, M., Golding, T. M., and Smith, G. S. (2020). Recent advances in the biological investigation of organometallic platinum-group metal (Ir, Ru, Rh, Os, Pd, Pt) complexes as antimalarial agents. *Molecules* 25, 5276. doi:10.3390/molecules25225276
- McMullen, M., Madariaga, A., and Lheureux, S. (2021). New approaches for targeting platinum-resistant ovarian cancer. *Semin. Cancer Biol.* 77, 167–181. doi:10.1016/j.semcancer.2020.08.013
- Meier-Menches, S. M., Gerner, C., Berger, W., Hartinger, C. G., and Keppler, B. K. (2018). Structure-activity relationships for ruthenium and osmium anticancer agents towards clinical development. *Chem. Soc. Rev.* 47, 909–928. doi:10.1039/c7CS0323C
- Melchart, M., and Sadler, P. J. (2006). Ruthenium arene anticancer complexes. In: Bioorganometallics. G. Jaouen, editor. Boschstraße, Weinheim: Wiley-VCH Verlag GmbH and Co. KGaA. p. 39–64.
- Mello-Andrade, F., Cardoso, C. G., Silva, C. R. E., Chen-Chen, L., Melo-Reis, P. R., Lima, A. P., et al. (2018). Acute toxic effects of ruthenium (II)/amino acid/diphosphine complexes on Swiss mice and zebrafish embryos. *Biomed. Pharmacother.* 107, 1082–1092. doi:10.1016/j.biopha.2018.08.051
- Mihajlovic, K., Milosavljevic, I., Jeremic, J., Savic, M., Sretenovic, J., Srejovic, I. M., et al. (2020). Redox and apoptotic potential of novel ruthenium complexes in rat blood and heart. *Can. J. Physiol. Pharmacol.* 99, 207–217. doi:10.1139/cjpp-2020-0349
- Milheiro, S. A., Gonçalves, J., Lopes, R., Madureira, M., Lobo, L., Lopes, A., et al. (2020). Half-sandwich cyclopentadienylruthenium(II) complexes: a new antimalarial chemotype. *Inorg. Chem.* 59, 12722–12732. doi:10.1021/acs.inorgchem.0c01795
- Mukherjea, D., Dhukhwa, A., Sapra, A., Bhandari, P., Woolford, K., Franke, J., et al. (2020). Strategies to reduce the risk of platinum containing antineoplastic drug-induced ototoxicity. *Expert Opin. Drug Metab. Toxicol.* 16, 965–982. doi:10.1080/17425255. 2020.1806235
- Nabiyeva, T., Marschner, C., and Blom, B. (2020). Synthesis, structure and anti-cancer activity of osmium complexes bearing π -bound arene substituents and phosphane Co-Ligands: a review. *Eur. J. Med. Chem.* 201, 112483. doi:10.1016/j.ejmech.2020.112483
- Nagy, E., Balogi, Z., Gombos, I., Akerfelt, M., Björkbom, A., Balogh, G., et al. (2007). Hyperfluidization-coupled membrane microdomain reorganization is linked to activation of the heat shock response in a murine melanoma cell line. *Proc. Nat. Acad. Sci. U. S. A.* 104, 7945–7950. doi:10.1073/pnas.0702557104

Omer, P. K., Aziz, N. M., and Omer, R. A. (2024). Comprehensive review of metal-based coordination compounds in cancer therapy: from design to biochemical reactivity. *Rev. Inorg. Chem.* 44, 699–710. doi:10.1515/revic-2024-0030

Pivarcsik, T., Pósa, V., Kovács, H., May, N. V., Spengler, G., Pósa, S. P., et al. (2022). Metal complexes of a 5-nitro-8-hydroxyquinoline-proline hybrid with enhanced water solubility targeting multidrug resistant cancer cells. *Int. J. Mol. Sci.* 24, 593. doi:10.3390/ijms24010593

Prathima, T. S., Choudhury, B., Ahmad, G. M., Chanda, K., and Balamurali, M. M. (2023). Recent developments on other platinum metal complexes as target-specific anticancer therapeutics. *Coord. Chem. Rev.* 490, 215231. doi:10.1016/j.ccr.2023.215231

Saha, S., Kushwaha, R., Mandal, A., Singh, N., and Banerjee, S. (2025). Recent advances in Rh(III)-based anticancer complexes. *Coord. Chem. Rev.* 525, 216306. doi:10. 1016/j.ccr.2024.216306

Singh, A. K., Kumar, A., Singh, H., Sonawane, P., Pathak, P., Grishina, M., et al. (2023). Metal complexes in cancer treatment: journey so far. *Chem. Biodivers.* 20, e202300061. doi:10.1002/cbdv.202300061

Sipos, A., Ujlaki, G., Mikó, E., Maka, E., Szabó, J., Uray, K., et al. (2021). The role of the microbiome in ovarian cancer: mechanistic insights into oncobiosis and to bacterial metabolite signaling. *Mol. Med.* 27, 33. doi:10.1186/s10020-021-00295-2

Skehan, P., Storeng, R., Scudiero, D., Monks, A., McMahon, J., Vistica, D., et al. (1990). New colorimetric cytotoxicity assay for anticancer-drug screening. *J. Natl. Cancer Inst.* 82, 1107–1112. doi:10.1093/jnci/82.13.1107

Son, M. H., Kim, J. Y., Lim, E. J., Baek, D. J., Choi, K., Lee, J. K., et al. (2013). Synthesis and biological evaluation of 2-(arylethynyl)quinoline derivatives as mGluR5 antagonists for the treatment of neuropathic pain. *Bioorg. Med. Chem. Lett.* 23, 1472–1476. doi:10.1016/j.bmcl.2012.12.056

Štarha, P. (2025). Anticancer iridium(III) cyclopentadienyl complexes. *Inorg. Chem. Front.* 12, 897–954. doi:10.1039/d4qi02472a

Štarha, P., and Trávníček, Z. (2019). Non-platinum complexes containing releasable biologically active ligands. *Coord. Chem. Rev.* 395, 130–145. doi:10.1016/j.ccr.2019.06.001

Wilkinson, B. L., Bornaghi, L. F., Poulsen, S. A., and Houston, T. A. (2006). Synthetic utility of glycosyl triazoles in carbohydrate chemistry. *Tetrahedron* 62, 8115–8125. doi:10.1016/j.tet.2006.06.001

Wu, W., Seeki, K.-i., and Kawazoe, Y. (1995). Effect of fluorine-substitution on basicity of benzo[h]quinoline, benzo[f]quinoline and quinoline. *Heterocycles* 41, 315–322. doi:10.3987/com-94-6940

Xu, Z., Kong, D., He, X., Guo, L., Ge, X., Liu, X., et al. (2018). Mitochondria-targeted half-sandwich ruthenium^{II} diimine complexes: anticancer and antimetastasis via ROS-mediated signalling. *Inorg. Chem. Front.* 5, 2100–2105. doi:10.1039/C8OI00476F.

Yu, C., Wang, Z., Sun, Z., Zhang, L., Zhang, W., Xu, Y., et al. (2020). Platinum-based combination therapy: molecular rationale, current clinical uses, and future perspectives. *J. Med. Chem.* 63, 13397–13412. doi:10.1021/acs.jmedchem.0c00950

Yufanyi, D. M., Abbo, H. S., Titinchi, S. J. J., and Neville, T. (2020). Platinum(II) and ruthenium(II) complexes in medicine: antimycobacterial and anti-HIV activities. *Coord. Chem. Rev.* 414, 213285. doi:10.1016/j.ccr.2020.213285

Zékány, L., and Nagypál, I. (1985). "Computational methods for the determination of formation constants," in *Computational methods for the determination of formation constants*. Editor D. J. Leggett (New York, NY: Springer Science and Business Media. p. 291–353.

Zeng, L., Gupta, P., Chen, Y., Wang, E., Ji, L., Chao, H., et al. (2017). The development of anticancer ruthenium(II) complexes: from single molecule compounds to nanomaterials. *Chem. Soc. Rev.* 46, 5771–5804. doi:10.1039/C7CS00195A

Zhang, C., Xu, C., Gao, X., and Yao, Q. (2022). Platinum-based drugs for cancer therapy and anti-tumor strategies. *Theranostics* 12, 2115–2132. doi:10.7150/thno. 69424

Zhang, H., Wang, Y., Thürmer, R., Parvez, K., Choudhary, I., Rahman, A.-u., et al. (1999). Neighbouring group participation of C-6 substituents of glucose derivatives on the stereoselectivity of the *N*-glycosidic linkage of glycopeptides. *Z. Naturforsch. B* 54, 692–698. doi:10.1515/znb-1999-0519